12-2019

Design and Testing of a Modular Laser System with Laser Machining and Bioprinting Capabilities

Jesus Gonzalez
The University of Texas Rio Grande Valley

DESIGN AND TESTING OF A MODULAR LASER SYSTEM WITH LASER MACHINING AND BIOPRINTING CAPABILITIES

A Thesis

by

JESUS GONZALEZ

Submitted to the Graduate College of
The University of Texas Rio Grande Valley
In partial fulfillment of the requirements for the degree of

MASTER OF SCIENCE IN ENGINEERING

December 2019

Major Subject: Manufacturing Engineering

DESIGN AND TESTING OF A MODULAR LASER SYSTEM WITH LASER MACHINING AND BIOPRINTING CAPABILITIES

A Thesis
by
JESUS GONZALEZ

COMMITTEE MEMBERS

Dr Jianzhi Li
Chair of Committee

Dr. Andrew Tsin
Committee Member

Dr. Ben Xu
Committee Member

December 2019

ABSTRACT

Gonzalez, Jesus., Design and Testing of a Modular Laser System with Laser Machining and Bioprinting Capabilities. Master of Science in Engineering (MSE), December 2019, 80 pp., 8 tables, 28 figures, 34 references, 27 titles.

This thesis introduces the applications of ultrafast lasers while focusing on their bioprinting capabilities. A custom system was designed to utilize a femtosecond laser for 2D and 3D applications. The characteristics of lasers allow them to be efficiently used in machining, 3D printing, research, and more. Their power and precision allow them to be used for delicate work such as bioprinting. Bioprinting is a field holding great potential to benefit society. Studies conducted over the years prove its usefulness in printing cells and biomaterials, while showing there is still much to improve upon before being able to print fully functioning organs.

The study found successful implementation of the laser system design. Etching and cutting experiments of different patterns on metals and non-metals were successful in the micrometer range. Bioprinting wise, the experiment was inconclusive with the parameters and visual analyses equipment used. No droplets were viewed, but lack of surveillance at the laser-bioink interface would be needed to verify the results. Future work is needed in surveilling the laser-bioink interface, adjusting the bioink with cells and collagen, creating a controlled environment, and lowering the pulse fluence.

DEDICATION

I would like to dedicate my master's thesis to my family and my partner, whose unconditional love and support have helped me throughout my entire higher education journey. My parents, my siblings, my twin brother Julian Gonzalez, and my girlfriend Alexandria inspired and supported me every step of the way. Achieving my degree would not have been possible without them.

ACKNOWLEDGEMENT

I would like to thank all the people who helped me in completing my thesis work. I give my thanks to Dr. Jianzhi Li, my academic supervisor, for his assistance and help during my higher education path. I would also like to extend my thanks to Dr. Ben Xu, who was part of my committee and provided me with academic feedback. Dr. Andrew Tsin also served in my committee and assisted in understanding the biological aspect of my thesis work.

I offer my thanks to Neal Linhart for helping me set up and maintain the laser system and corresponding software. The time and complications associating with building the system was significantly reduced through his help.

I am thankful for the resources and assistance provided by the engineering department and Dr. Rajiv Nambiar. Elizabeth Rodriquez, from the manufacturing department, also greatly helped me.

I would also like to extend my thanks to the other graduate members of Dr. Jianzhi Li's lab group. Special thanks go to Chaoran "Henry" Dou for assisting in testing and setting up the laser system and Victoria Perez for aiding in biomaterial preparation and biological understanding.

TABLE OF CONTENTS

Page

ABSTRACT…….....iii

DEDICATION…….....iv

ACKNOWLEDGEMENTS…….....v

TABLE OF CONTENTS…….....vi

LIST OF TABLES……..ix

LIST OF FIGURES…….x

CHAPTER I. INTRODUCTION AND BACKGROUND INFORMATION…….1

1.1 Chapter Overview……..1

1.2 Lasers…….....1

1.3 Laser Micromachining……...3

1.4 Bioprinting…….....6

1.5 Problem Statement ……8

1.6 Research Objectives...……9

1.7 System Overview……...9

CHAPTER II. LITERATURE REVIEW ……11

2.1 Chapter Overview……....11

2.2 Biomaterials……11

2.3 Spin Coating……..….....12

2.4 Laser Based Bioprinting…….....14

2.5 Laser Induced Forward Transfer (LIFT)……15

CHAPTER III. RESEARCH METHODOLOGY……17

3.1 Chapter Overview……17

3.2 System Equipment…….....17

3.3 System Design……22

3.4 Structural Integrity Test…….....24

3.5 General Setup and Design……....25

CHAPTER IV. EXPERIMENTAL SETUP AND RESULTS…….....27

4.1 Chapter Overview……27

4.2 Laser Micromachining……27

4.3 Alginate Mixture……...……...33

4.4 Spin Coating: Alginate Mixture……...35

4.5 Ribbon……...……...38

4.6 Design of Experiments…….40

4.7 Results and Analysis……43

CHAPTER V. CONCLUSION……...……...49

5.1 Chapter Overview ……...49

5.2 Results……..49

5.3 Future Work…….…50

REFERENCES……..….52

APPENDIX……57

BIOGRAPHICAL SKETCH……...……...……...80

LIST OF TABLES

Page

Table 3.1: Sprit One 1040-8 Specifications……...……18

Table 4.1: Alginate Properties……..….34

Table 4.2: Solution Percentages……...…..…35

Table 4.3: Solution Density……...35

Table 4.4: Four Factors with Four Levels……..40

Table 4.5: Laser Power in Watts……41

Table 4.6: Experimental Results……45

Table 4.7: Laser Fluences Created by the 4x4 Power to Pulse Array……48

LIST OF FIGURES

Page

Figure 1.1 Schematic of possible laser material processes…….…….2

Figure 1.2 General schematic for laser based bioprinting processes……...7

Figure 2.1 Spin Coating Process Schematic…….....13

Figure 2.2 Single Cell Isolation experiment conducted on Hela cells……...16

Figure 3.1 Spirit one laser used in the system……...19

Figure 3.2 Beam expander used in the system……...19

Figure 3.3 Galvanometer from Aerotech……...21

Figure 3.4 Galvanometer to Z stage Composition…….21

Figure 3.5 Optical Table used in the System (Newport)……...22

Figure 3.6 Final CAD model of the system designed in SolidWorks……23

Figure 3.7 Current state of the physical setup……24

Figure 3.8 Deflection Distribution with 750N……...25

Figure 4.1 Initial Software Interface……..28

Figure 4.2 Beam Route Schematic……30

Figure 4.3 Software Interface……31

Figure 4.4 Etching Examples on Aluminum/Steel Sheets……32

Figure 4.5 Zoomed in View of Cut on Aluminum Foil……..…33

Figure 4.6 Sodium Alginate Solutions……...36

Figure 4.7 Spin Coater……...36

Figure 4.8 High Precision Scale……..…37

Figure 4.9 Quartz Disc with a Bioink Layer……..38

Figure 4.10 Donor Substrate Section (a), Receiving Substrate Section (b), and Full Ribbon (c).39

Figure 4.11 Separation Between Donor and Receiving Substrates without Bioink Layer……40

Figure 4.12 Spectra Physics Advanced Screen……..41

Figure 4.13 Laser Sequence Array, Laser Power Vs. Laser Pulses……...42

Figure 4.14 Optical Microscope……43

Figure 4.15 Magnification of Holes Created with the Original Number of Laser Pulses…….44

Figure 4.16 Pulse Firing Event Data Capture……....46

CHAPTER I

INTRODUCTION AND BACKGROUND INFORMATION

1.1 Overview of this Chapter

This chapter introduces background information on topics that will be studied in the following chapters. Sections 1.2 and 1.3 gives general information on lasers and some of its applications. Section 1.4, its subsections, shows information on bioprinting, types of bioprinting, as well materials used in bioprinting. Sections 1.5 and 1.6 introduces the objective of this paper while section 1.7 gives a brief overview of the system utilizing a laser for various purposes.

1.2 Lasers

Lasers, an acronym for light amplification by stimulated emission of radiation, are essentially a homogenous group of light with the same wavelength traveling along a tight, uniform path [1]. There are many kinds of lasers which can be categorized in various manners depending on which property of the laser one looks at. Based on the physical state of the medium, there are solid, gas, liquid, and the special free-electron lasers [2]. They can be categorized based on their wavelength, such as infrared, visible, ultraviolet, and x-ray lasers [2]. There are also categorizations based on time, separating lasers based on whether they are continuous or pulsed, the latter which is either short or ultrashort. [2]. These three categories combine to give the characteristics of a single laser, i.e. a solid state, infrared, short laser or a gas, ultraviolet, continuous laser. The range in combinations that make up lasers allow them to

be a very versatile tool which can be used for various purposes. These combinations are enhanced even more when looking at the ranges of the individual components in these categories. For instance, when speaking of the wavelength, if a laser is an infrared laser, it could be near infrared, mid infrared, or infrared, where each subsection has a range along the light spectrum. Regarding the physical state, each state has numerous materials to choose from, different solids and gases available, making the list of possible combinations even longer. Each has its own advantages disadvantages, meaning that choosing the right one could be daunting, but in general, depending on the type, most can be interchanged depending on the project. They have been used in a wide range of projects: polishing [3], micromachining, micro electromechanically systems (MEMS), microelectronics [4], microfluidics [5] biochemical sensing [6], general machining shown in Fig 1.1 [7], bioprinting, and much more due to their varying parameters.

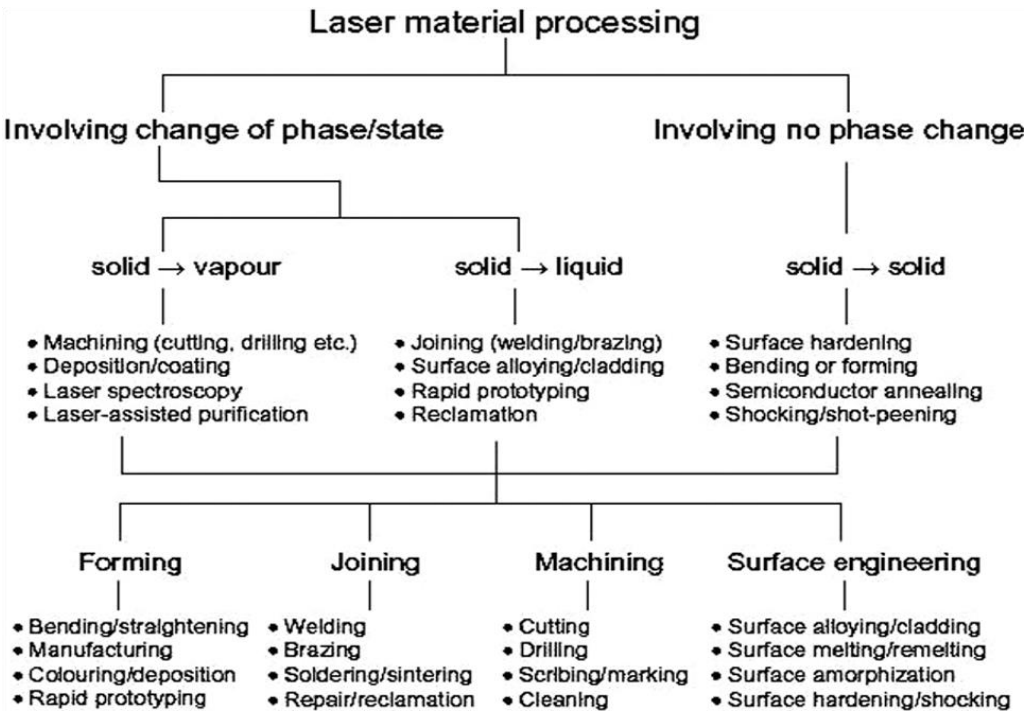

Figure 1.1 Schematic of possible laser material processes [7]

1.3 Laser Micromachining

Laser beam micromachining (LBMM) utilizes laser to machine on the micro scale. It accomplishes the same as laser beam machining (LBM), except on much smaller tolerances. It essentially a micro version of LBM which means that it includes micro version of all the LBM processes, such as laser beam drilling (LBD), laser beam cutting (LBC), laser beam turning (LBT), and so on [8]. LBMM is mostly a material removing process where short and ultrashort (or fast and ultrafast) lasers are used with wavelengths varying from UV (ultraviolet) to IR (infrared) depending on the material and application. Ultrafast lasers are used do to the fact that the time scale is small enough to avoid any collateral damage that could be caused by the heat of the laser, essentially reducing the heat affected zone. Metals, insulators and semiconductors, ceramics, and polymers are a few of the materials able to be worked on through LBMM [8].

The outcome of the processes in LBMM are influenced by various laser parameters listed below [7] [9]:

- Laser Power (P)
    - P is the average power output of the specific laser.
- Laser Wavelength (λ)
    - Measured as the distance between two consecutive peaks of a wave at a certain frequency. It has been studied to see which wavelengths lead to smaller spot size as well as whether longer or shorter wavelengths give better surface quality.
- Pulse repetition frequency (PRF)/Repetition rate

- Pulses per second that the laser is firing. Studies show that high PRF ensures uniform heat accumulation and its effect on structures and ablation among other things have been studied as well.

- Laser Pulse Width (τ)
  - Time duration of the pulse. The shorter the pulse width equates to shorter times for heat to spread from the lasers contact with the material, therefore leading to smaller heat-affected zones.
- Translation Speed (U)
  - This is the linear speed of the material being worked on relative to the laser spot focus.
- Pulse Energy
  - E_p is the average power per pulse of the laser. Research has shown that higher pulse energies lead to greater ablation volumes.

$$E_p = \frac{P}{PRF} \tag{1}$$

- Peak Power
  - P_{peak} is the laser's peak power.

$$P_{peak} = \frac{E_p}{\tau} \tag{2}$$

- Laser Intensity (I)
  - I is the intensity of the laser at the focal spot.

$$I = \frac{P}{\pi * D^2} \tag{3}$$

- Where D is focal spot radius

- Pulse Fluence (F_p)
  - Pulse fluence is the laser pulse energy per unit area of the focal spot. Fluence affects both the absorption mechanism of materials as well as the threshold for ablation, where even small fluences can cause ablation in certain materials.

$$F_p = \frac{E_p}{\pi * D^2} \tag{4}$$

    - Accumulated fluence: the total fluence after N number of pulses

$$F_{acc} = N * F_p \tag{5}$$

- Focal Spot Size (D)
  - D is the radius of the focused spot size of the laser. It is the radius after the laser has been focused using lens.

$$D = \frac{2 * \lambda * f}{\pi * w} \tag{6}$$

  - Where f is focal length of the lens and w is beam radius at lens inlet
  - Two factors important to the focal spot are focal length and depth of focus
    - Focal length: distance from lens to focal spot, a constant of the lens
    - Depth of focus: depth of field inversely proportional to numerical aperture

$$Depth\ of\ focus = \frac{\pi * D}{\lambda} \tag{7}$$

There are other factors besides the laser parameters that determine the outcome of the process. These include material type, focusing method, number of passes, and the number of pulses [7]. Material properties differ from material to material meaning the effect of lasers on them differ as well due to parameters like absorptivity, reflectivity, thermal properties and so on. How the laser is focused adjusts the energy and intensity reaching the medium affecting how it is damaged. The number of pulses has a similar effect as the PRF when it comes to ablation. All these factors affect the LBMM processes as well as other processes lasers can be used for.

1.4 Bioprinting

Bioprinting is the printing of biological materials. It is the process of precisely depositing biological materials, or cells in biomaterials, into three dimensional structures utilizing 3D bioprinting equipment [10] [11]. The applications for such a technology are vast, especially in the medical field. There have been studies on its applications on tissue engineering [12], single cell isolation [13], tissue models for drug discovery [14], and much more. There exist various methods for bioprinting which are discussed in section 1.4.1 and 1.4.2.

1.4.1 Non-Laser Based Bioprinting

There are various non-laser based bioprinting methods used for research. These include, but are not limited to, droplet-based bio printing, extrusion-based bioprinting [14], micropatterning, ink-jet printing, nanocontact bioprinting [15], and cell ball assembling bioprinting [11] are some of the processes which can also be split into direct contact or direct write methods. Methods such as extrusion-based or droplet-based/ink-jet printing are much like their non-biological manufacturing counterparts where a filament is extruded in extrusion based, but it contains biological components, and droplets are used to print in the droplet-based/ink-jet

except instead of ink, bioink is used. These are direct write, or “bottom-up techniques” [15] whereas methods like micropatterning, a direct contact method, use a sort of stamp coated with the bioink to place the media on the desired substrate all at once.

1.4.2 Laser Based Bioprinting

There are four main/common laser based bioprinting methods: laser-induced forward transfer (LIFT), absorbing film-assisted LIFT (AFA-LIFT), biological laser processing (BioLP), and matrix-assisted pulsed-laser evaporation direct write (MAPLE-DW) [15]. They all essentially use the same base structure setup seen in Figure 1.2, an optically transparent ribbon, a coated receiving substrate, beam optics, and a laser system along with various auxiliary equipment like imaging device and computer-controlled stages. The core differences are their variations in ribbon make-up and laser wavelengths.

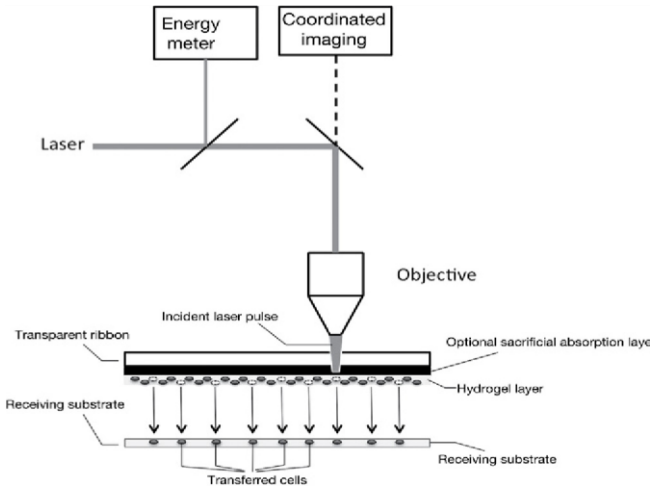

Figure 1.2 General schematic for laser based bioprinting processes [15].

Between LIFT and AFA-LIFT, a core difference is in the metal film in the ribbon. Where LIFT uses a dynamic release layer, AFA-LIFT uses a thicker metal film to protect the cells from laser damage. AFA-LIFT is simply a modified version of LIFT in this sense, so the processes are

very similar. It is the parameters of some of the materials and equipment which are different. LIFT is a process with high resolution printing of small amounts of solid or liquid materials [16]. A large range of materials can be utilized in LIFT and printed down to a few micrometers. The process uses the heat absorption from a laser to create a vapor bubble at the film/coating interface that expands to the surface to create a jet to form a droplet on the receiving substrate. When a metal film is involved, the increase in pressure and temperature not only causes a vapor bubble, but for the thin film to break in a shock wave that could damage some of the cells. The thermal damage as well as the hydrodynamics of the bubble depend on the type of laser as well as the laser fluence. The size of the droplets depends on the thickness of the film, it's properties, and the property of the bioink: their density, viscosity, and surface tension to name a few. LIFT has been used to print liposomes, DNA [30], cDNA [29] proteins, nanotubes, metals, inks, and more [16].

1.5 Problem Statement

Previous experiments have been conducted in laser based bioprinting with various objectives in mind and with varying successes. These experiments vary from isolating single cells using LIFT [13], studying jet/droplet formation of different bioink due to cell presence [17], examining LIFT of liquids in bioprinting [18] and more. These had different objectives with different experimental setup, but all helped progress a part of the topic that is bioprinting and its capabilities. For the initial step, the purpose of this proposal is not to test out the parameters of a certain bioink solution with cells to ensure viability, nor to print living tissue. Instead, it is testing the capabilities of a designed modulated laser system and its ability to conduct bioprinting experiments by first performing a base experiment to find the optimal printing parameters for a cell-less bioink solution utilization varying ribbon and laser parameters.

1.6 Research Objective

As previously mentioned, the purpose of this study is to introduce applications of ultrafast lasers with a focus on their bioprinting capabilities as well as create a system to test out and apply these topics. To accomplish this, a system is needed that can utilize a capable laser and auxiliary equipment in an efficient and modular manner in order to adjust to various projects and needs requiring different parameters and setups. This system should allow for 2D and 3D experimentation of a variety of materials including bioink, which will be the material used in the first experiment the system is a part of. The main objectives of this study are listed below:

- To design a modular system with a laser power source utilizing already owned equipment and any other auxiliary equipment for use in various projects
- To choose suitable materials for the system's base and cage to ensure a safe and stable setup along
- To build and test the system to ensure it is in safe working condition to begin experimental usage
- To verify the system's bioprinting capabilities by using LIFT to find the optimal parameters with which to print cell-less bioink

1.7 System Overview

The system is built around a class 4 infrared femtosecond laser. The movement of the system consists of three linear stages, X, Y, and Z. The laser beam travels through a beam expander, redirected horizontally and vertically by optical mirrors, and enters a galvanometer before reaching its destination. The cage is made of 80/20 aluminum bars with a lower and upper level. The lower level contains the stages, galvanometer, as well as the columns which hold up

the second level. The second level holds the laser, beam expander, and optics on top of an optical board. The entirety of it rests a top a vibration dampening optical table. A more detailed look at the equipment, design, and final setup can be found in Chapter III.

CHAPTER II

LITERATURE REVIEW

2.1 Overview of this Chapter

This section reviews biomaterials and several studies in bioprinting performed utilizing a variety of laser-based methods while focusing on experiment closely related to the LIFT process.

2.2 Biomaterials

Biomaterials are any biological material found in nature and are used in bioprinting to encapsulate and hold the cells, though studies have been done on cell-less biomaterials as well, or cell-less bioink to be more exact. Bioink can be divided into two main types: scaffold-based and scaffold-free bioink [10]. In scaffold-based, cells are placed into external biological mediums, like hydrogels, to be printed onto a 3D receiver, whereas in scaffold-free printing, there is no external biological medium involved. Both types contain biomaterials with varying properties useful for different processes.

Scaffold-based biomaterials include hydrogels, decellularized matrix components, and microcarriers. Hydrogels makes up most of the materials and are substances that can absorb and retain large amounts of water. They are split into natural and synthetic hydrogels, where the former can be split by where the material is derived from, i.e. taken from the vertebrae and so on. Both natural and synthetic hydrogels have advantages and disadvantages to each other. For instance, natural hydrogels are weaker than synthetic hydrogels mechanically, but synthetic

hydrogels lack some signaling components found in natural hydrogels. Some hydrogels used in bioprinting include, but not limited to, alginate, chitosan, fibrin, gelatin, and synthetics materials like methacrylated gelatin and poly (ethylene glycol). Scaffold-free biomaterials include tissue spheroids, cell pellets, and tissue strands. The choice of bioink is heavily based on the process and the material properties of the biomaterial. Many of these are compared to through criteria like bioprintability, compatibility with bioprinting process, cell viability, affordability, scalability, mechanical and structural integrity, and more [10].

2.3 Spin Coating

Bioprinting processes and applications often require biomaterials to be deposited onto flat or smooth surface substrates through spin coating: a type of film deposition device used to create very thin layers. The bioink, or coating material, is placed in the center of a substrate that is already located on the spin coating device platform beforehand. Once operated, the spin coater will spin at high speeds and the resulting outward force will disperse the material uniformly throughout the substrate surface. The device continues to rotate until the user's desired thickness is achieved, which lowers as more material is evaporated or propelled from the outer edge (s) of the substrate. The thickness of the thin film of biomaterial is dependent on the material properties, such as viscosity and density, and processing parameters: rotation speed, spin time, and substrate material [19]. Within the past decade, spin coating devices have been implemented to produce thin films of indium oxide, ZnO, titanium oxide, and conducting oxides [19]. Yusuf et al. (2018) achieved a 300nm film thickness by repeatedly coating 1 ml of NiZn ferrite solution onto an indium tin oxide (ITO) glass substrate and setting the spin coater to operate at 3500rpm for 25s under room temperature [20]. Zaharieva and Milanova (2017) produced several SiO2 and

composite films by utilizing 0.5 ml of solution and a KW-4A spin coater and operating the device between 20-60 s at a rotation speed of 2000-6000 rpm [19].

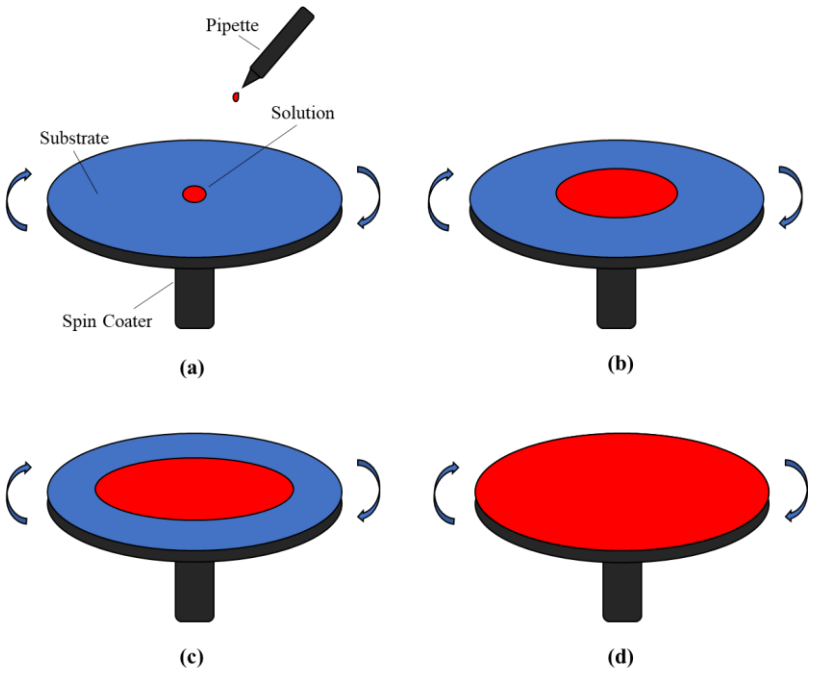

Figure 2.1 Spin Coating Process Schematic

The spin coating process can be divided into four main stages: deposition, substrate acceleration, substrate rotation at a constant rate, and deceleration [19]. A simplified schematic of the process can be observed in Figure 2.1, where the blue represents the substrate surface, the red represents the solution, and the arrows indicate the direction of the rotation for the spin coating device. During the first stage, a deposition device such as a digital pipette, is utilized to transfer a certain amount of solution onto the center of the substrate. The substrate, at this point, can be turned on at a low speed to facilitate flow for higher viscosity solutions. Once the higher speed is set, the spin coater accelerates until a constant rotation is achieved and the solution is evenly spread across the substrate. The final stage of the process involves the deceleration of the spin coater to a stop, during which evaporation of film starts occurring [20].

2.4 Laser Based Bioprinting

Laser based bioprinting has been used for a variety of experiments. This section shows a select few of these experiments with most of them being focused on LIFT based bioprinting.

The first experiment utilized matrix-assisted pulsed-laser evaporation direct write (MAPLE-DW) [15]. This method of laser printing, though containing a similar base structure to LIFT, is an “all-optical imaging and printing system with environmental controls” [15]. It was used to create a single cell 4x4 array pattern with spacing of 800μm center-to-center. This array was generated using MAPLE-DW where the biomaterial contained single MDA-MB-231 human breast cancer cells.

Biological Laser Printing (BioLP) has also been used to study the printing of cells for tissue engineering [12]. In this study, a ND: YAG crystal laser with a wavelength of 1064nm and power output of 7W was used to printing a sodium alginate solution, synthesized nano-sized hydroxyapatite (nano-HA), and human endothelial cells (EA.hy926). The experiments were carried out while studying the scanning speed of the galvanometer, laser fluence, and the ribbon to substrate gap distance. The parameters of the alginate solution were changed to adjust viscosity to obtain a favorable bubble formation without bursting as well as changes to the scanning speed to change from isolated droplet arrays to line patterns. AS for the nano-HA, it was found that increasing the laser fluence (400 to 500 mJ cm^{-2}) increased the droplet diameters and the forming of splashed droplets. For the EA.hy926 portion, laser fluence was tested as well as the capability to produce complex patterns thanks to the CAD/CAM workstation. Long term viability tests showed that viability of printed cells after incubation up to 11 days after their transfer [12].

Section 2.5 Laser Induced Forward Transfer (LIFT)

One experiment using LIFT studies the jet formation and properties of different biomaterial solutions at different laser fluences [17]. The experiment uses an argon fluoride (ArF) excimer laser with wavelength of 193nm to experiment, at varying laser fluences, on two different bio solutions: cell-free alginate/DMEM solution and cell-laden alginate/DMEM + 5 x 10e6 cells/mL, where DMEM is Dulbecco's Modified Eagles Medium which was used to culture fibroblasts. The study found that when laser fluences increased, the jet velocity, breakup length, and droplet size increased with a well define jet. It also found that when compared to cell-free bioink printing, the cell-laden transfer threshold is higher while the jet velocity, breakup length, and droplet size are lower, shorter, and smaller [17].

LIFT has been used to study the transfer of liquids, or bioinks. This experiment used a pulsed Nd: YAG laser with wavelength of 355nm to study the effects of laser pulse energy and film to substrate distance on a protein solution composed of 10mg/mL BSA (Sigma A1470) mixed with a water and glycerol at a 50% (v/v) concentration [18]. The tests used optical microscopy to measure the size and volume of the droplets. First droplets were printed at varying energies (55 to 400 nJ) at a constant film to substrate distance and then they were printed at varying film to substrate distances (0.03 to 5.0 mm) at three different energies (170, 360, and 630 nJ). A linear relationship was found between laser pulse energy and droplet value. For the film to substrate parameter, droplets were found for all energies at distances less than 0.5mm, while variations were found for all three energies above this value, splash, no droplet, non-uniform droplets [18].

LIFT is also capable of isolating single cells [13]. In this study, whose setup can be seen in Figure 2.2, HELA cells were printed utilizing a YAG pulsed laser at a wavelength of 535 nm.

Six single factor experiments were conducted with 25 laser pulses for each value of each factor to study their effect on the number of cells separated and the diameter of the separated cells at these 25 laser pulses. The six factors were: laser pulse energy, laser spot size, thickness of titanium, working distance, glycerol concentration with the medium, and alginate thickness on receiver. A three level, four factor orthogonal experiment was also conducted using the former four factors to optimize the cell isolation process by measuring the number of cells, peak size, and proliferation ratio. Their study concluded that the optimal settings for their experiment were: laser pulse energy = 9 μJ, spot size = 60μm, titanium thickness = 12nm, working distance = 700μm, glycerol concentration = 2-4%, and alginate thickness > 1 μm [13]. It also found that the two main factors were laser fluency and titanium thickness due to their influence over the energy introduced to the process.

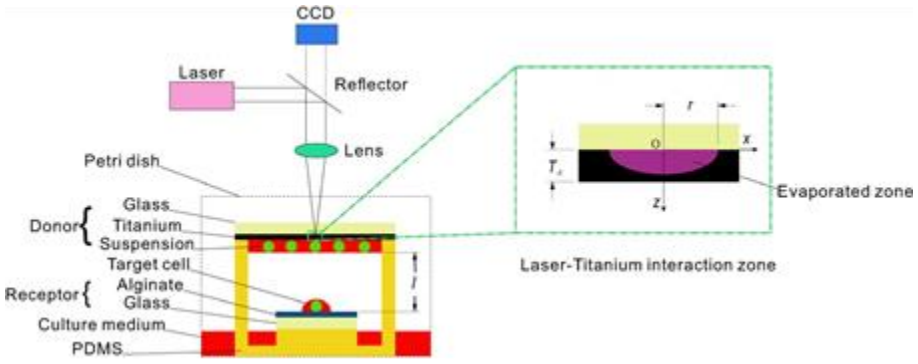

Figure 2.2 Single Cell Isolation experiment conducted on Hela cells [13]

CHAPTER III

METHODOLOGY

3.1 Overview of this Chapter

Chapter III details the entirety of the laser-based system. Section 3.2 introduces the various parts of the system, the laser, opto-mechanics, stages, etc. Sections 3.3 shows the design of the system as well as the current physical setup, the digital and real versions of the system. Section 3.4 explains the structural integrity test conducted digitally to confirm the effectiveness and feasibility of the design. Section 3.5 describes the general experimental setup of the project that will be conducted using the system, the materials, ribbon, and the design of the experiment.

3.2 System Equipment

The core of the design is centered around the Spirit One 1040-8 laser. It is a diode pumped solid state ytterbium (YAG) femtosecond laser. The laser is shown in Figure 3.1 while the specifications of the laser are found in Table 3.1. A chiller is included with the laser to maintain the cooling loop of the laser and avoiding overheating by keeping the system within operating temperatures. The physical details and voltage requirements of the chiller can also be seen in Table 3.1.

Table 3.1: Sprit One 1040-8 Specifications [31]

	Spirit One 1040-8	Spirit One 1040-8-SHG
Output Characteristics		
Wavelength	1040 ± 5 nm	
Output Power	>8 W	
Pulse Energy	>40 µJ at 200 kHz	
Wavelength (SHG)	NA	520 ± 3 nm
Output Power[2] (SHG)	NA	>4 W at 200 kHz
Pulse Energy[2] (SHG)	NA	>20 µJ at 200 kHz
Repetition Rates[3]	200 kHz or 1 MHz	
Pulse Selection	Integrated pulse picker (AOM) for single shot to 1 MHz operation	
Pulse Width	<400 fs	
Pulse Width Tunability[4,5]	400 fs to 4 ps; tunable by software	
Power Stability	<1% rms over 100 hours (for 1040 nm and 520 nm)	
Pulse-to-Pulse Stability	<2% rms	
Spatial Mode	TEM_{00}, M^2 <1.2	
Beam Diameter (at exit)	2.0 mm (1040 nm); 2.0 mm (520 nm)	
Beam Divergence	<1 mrad (1040 nm); <0.5 mrad (520 nm)	
Pre-Pulse Contrast Ratio	>250:1	
Polarization	Linear	
Cold Start Time	<30 min	
Warm Start Time	<15 min	
Environmental Specifications		
Operating Temperature	18–30°C (64–86°F)	
Humidity	<65%, non-condensing	
Cooling Requirements		
Laser Head	Closed-loop chiller, included with shipment	
Utility Requirements		
Voltage	Laser Head: 24 VDC Chiller: 100-240 V, 50/60 Hz	
Current	<15 A	
Laser Head Physical Characteristics		
Dimensions (L x W x H)	26.2 x 12.2 x 5.2 in (665 x 310 x 133 mm)	29.1 x 12.2 x 5.2 in (740 x 310 x 133 mm)
Weight	88 lb (40 kg)	99 lb (45 kg)
Closed Loop Chiller Physical Characteristics		
Dimensions (L x W x H)	19.0 x 15.8 x 10.5 in (484 x 400 x 267 mm)	
Weight	68 lb (31 kg)	

Figure 3.1 Spirit one laser used in the system [31]

The laser beam routing subsystem is comprised of a beam expander (seen in Figure 3.2), optical mirrors, and mirror mounts. The beam expander is a S6EXP0050/328 Sill OPTICS Beam Expander composed of fused silica with a low absorption coating rated for 1030-1090nm wavelength and 5.0x magnification. It can expand the 2mm beam diameter of the Spirit One laser up to 10mm. The 1" optical mirrors are held in place using a combination of Suprema 1"stainless steel mirror mounts, 45-degree mirror holders, v-block cylindrical device mounts, vertical rail posts, and optical mounting posts which aid in redirecting the beam horizontally and vertically.

Figure 3.2 Beam expander used in the system [32]

The motion subsystem consists of an XY stage, a Z stage, and a galvanometer with custom made attachments. They XY stage is a composite stage composed of an X stage, a PRO165LM-0150-TT1-E2-CMS2-PL0-TAS PRO165LM Mechanical-Bearing Direct-Drive Linear Stage with 150mm of travel, that sits below and is connected to a Y stage, a PRO115LM-150-TT1-E2-CMS4-PL0-TAS PRO115LM Mechanical-Bearing Direct-Drive Linear Stage with 150mm of travel. The objects to be worked on by the laser are mounted onto the Y stage portion of the XY composite. The Z stage is a PRO115SL-150-M2-3-LI1-CP1-PL0-TAS PRO115SL Mechanical-Bearing Screw-Driven Linear Stage with 150mm of travel. Mounted onto the Z stage is the galvanometer (seen in Figure 3.3), an AGV10HPO-BE1-W5-PL0-TAS AGV10xxx High-Performance Galvanometer Scanner with a 10mm aperture. The galvanometer, along with an S4LFT4065/328 telecentric F-Theta lens, is used to focus the beam from the laser such that it can be used for micromachining or bioprinting. The distance for optimal beam focusing with this setup is 83.1mm. The galvanometer is attached to the Z stage via a custom attachment designed and machined using 80/20 aluminum. A custom 3D printed attachment was also designed and created in order to allow the placement of an optical mount near the galvanometer to route the beam from a vertical direction to a horizontal one to enter the galvanometer. These attachments and the galvanometer to Z stage composition can be seen in Figure 3.4.

Figure 3.3 Galvanometer from Aerotech [33]

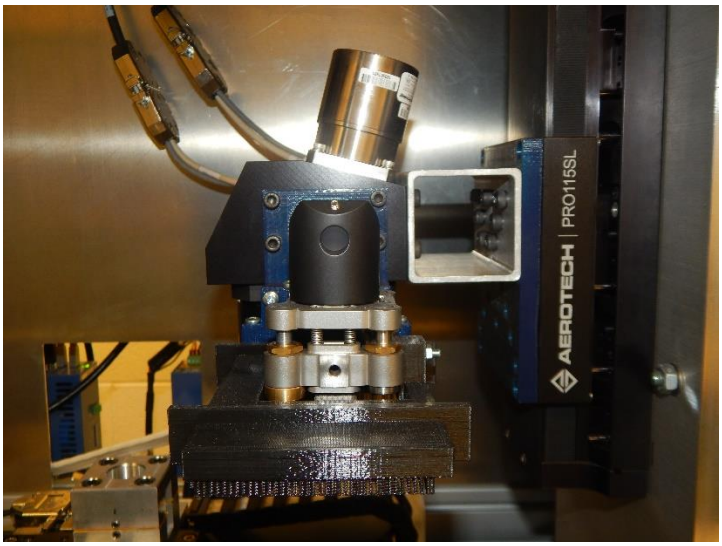

Figure 3.4 Galvanometer to Z stage Composition

80/20 aluminum bars, panels, and other auxiliary connectors, attachments, and fasteners were used to construct the frame, shell, and columns of the design. The entire construct is held atop of an Integrity 3, 900 x 1800 x 203 mm, Metric M6 holes, Isolated Optical Table (Figure 3.5). A 600x1200mm Optical breadboard with a custom hole for laser beam routing was also purchased for use as a base for the second level of the frame.

Figure 3.5 Optical Table used in the System (Newport) [34]

3.3 System Design

The system was designed around the laser and the stages to ensure ample room was available for the equipment on the optical table while keeping good stability. 80/20 aluminum bars were used to create the cage for the entire setup, which was designed to have two enclosed levels. The bottom level contains the XY and Z stage along with the galvanometer attached to the Z-stage and the custom attachment on the galvanometer to mount the optics. Also included are two vertical columns made by 1/2”and 1/4” thick aluminum plates from 80/20 Inc. whose purpose is to hold up the second level as well as to have the Z-stage attached to one vertically. On the second level lies the optical board acting as the floor for the second level. Attached to it are most of the optics and the beam expander as well as the Spirit One laser itself. Aluminum panels cover every wall of the cage, on the 1st and 2nd level, except for the front, where two doors made from the aluminum bars are located to allow access to the equipment. These doors are covered by acrylic panels. There is also a sliding door on the very top made of aluminum bars and an aluminum panel to allow access to the optics and the laser from above. The drivers for the

stages and the galvanometer are located outside of the cage, bolted onto the optical table and are connected by their respective wires through a hole in one of the aluminum panels. The laser is connected to the chiller located to the side of the optical table. Both the laser and the drivers are connected to a laboratory specific PC containing the software that controls them. Basic physics calculations were applied to ensure the cage could handle the weight of the laser. The system was designed and redesigned to account for the addition of equipment. The final CAD design can be seen in Figure 3.6 and the physical design can be seen in Figure 3.7.

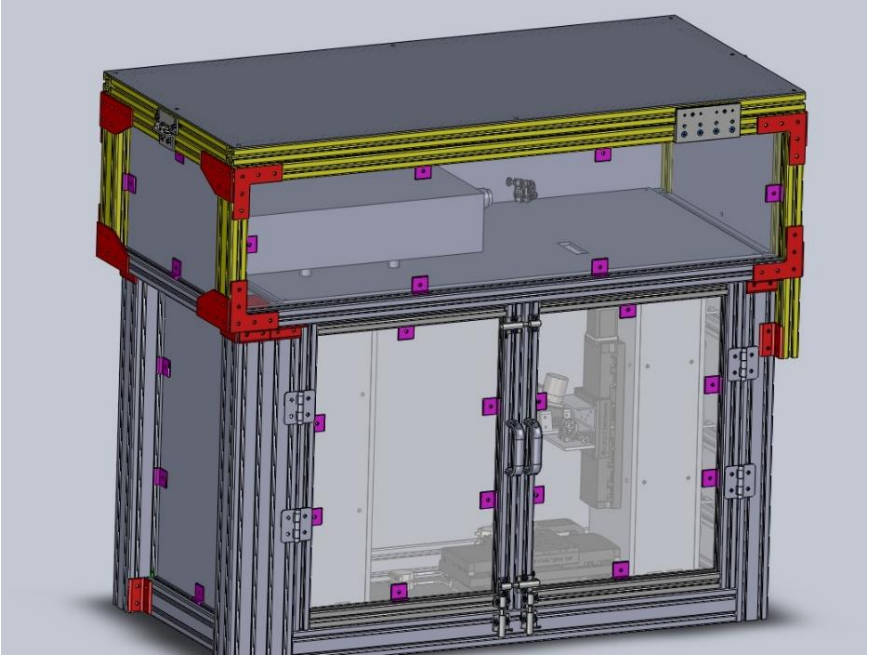

Figure 3.6 Final CAD model of the system designed in SolidWorks

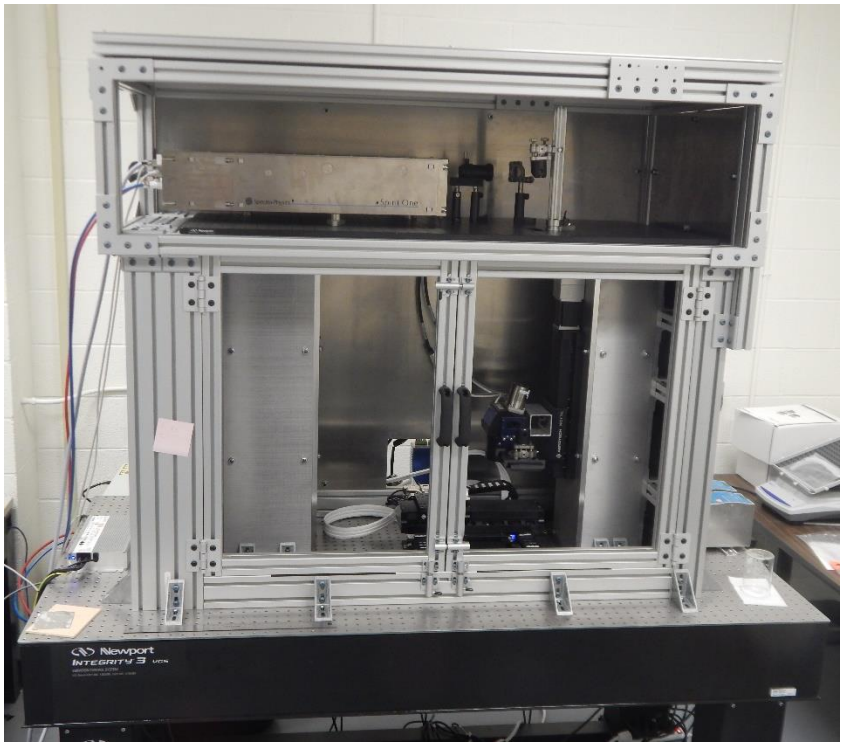

Figure 3.7 Current state of the physical setup

3.4 Structural Integrity Test

Before finalizing the design, structural analysis was conducted on a simple, earlier version of the design to ensure structural stability. This earlier design did not include the two vertical columns, whose purposes were to one, hold the Z stage in place on a vertical surface, and two, reinforce the 2nd story of the structure, more importantly, the area of the 2nd story where the Spirit One laser would be placed.

The deformation test was conducted in SolidWorks Simulation utilizing the static simulation module. Since the 6105-T5 grade aluminum that composes the 80/20 aluminum bars is not an option for material use, the material that had the closest modulus of elasticity and yield strength, 70,326.5 N/Sq. mm and 241.1N/Sq. mm respectively, was chosen as the material for the study. The chosen material was a 6063-T83 Aluminum alloy with a modulus of elasticity of

69000 N/Sq. mm and a yield strength of 240 N/Sq. mm. The force applied in the study was 750N, which was composed using 10m/s^2 for gravity and the 40kg weight of the Spirit One laser as well as an overestimated 35kg weight for everything in the second level. The simulation returned a maximum displacement of 0.1378mm. The deflection distribution can be seen in Figure 3.8 which shows the deflection returned by the simulation. Considering the size of the structure, as well as the lack of reinforcement the final design contains with regards to the two vertical columns, the deflection due to the force applied by the weight is negligible.

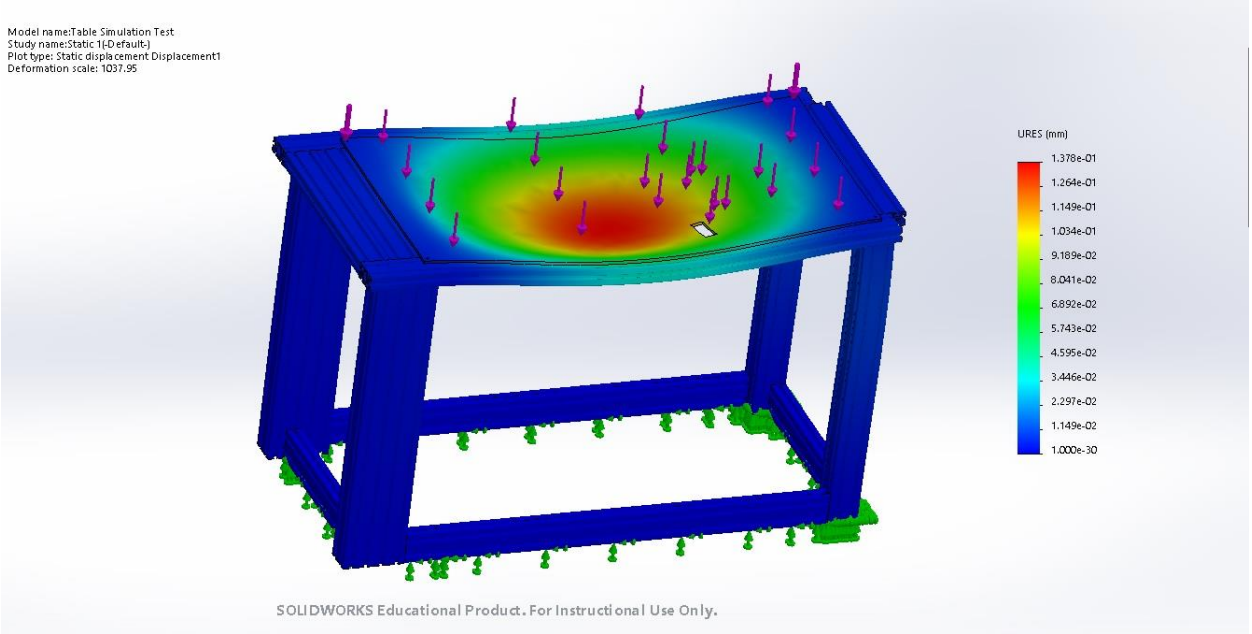

Figure 3.8 Deflection Distribution With 750N

3.5 General Setup and Design

For the purpose of this study, the experiment will not involve cell-laden bioink as it will be a test experiment to see the capabilities of the system and how it handles cell-less bioinks. The experiment will be a 4-factor factorial experiment testing the concentrating of a sodium alginate with water solution to be used as the bioink, the thickness of the bioink layer in the ribbon, the

power of the laser, and the pulse rate of the laser as well. It may test more than these four factors if the need arises, such as linear printing speed and working distance, but the former four factors would be the initial focus. The response variable would be the corresponding droplet shape and size along with any non-homogeneous droplets, i.e. uncontrolled splash of the bioink. Depending on the equipment, a high-speed camera will be used to create a time lapse of the process for each droplet to study the physical action of them dropping and whether it is controlled or not. The samples will be studied using a Seismic Electron Microscope (SEM) to visually be able to the see the micrometer sized droplets, measure them, and see whether the process was successful or not. If the SEM cannot be used, an optical microscope will be used in its place.

The ribbon that will be used will be compromised of fused silica, or quartz glass, that will act as the donor substrate. A thin layer of the chosen bioink composition will be coated on to the quartz glass. For the receiving substrate, quartz glass will also be used, or a high-grade petri dish. On the glass may be a thin layer of a different biomaterial to help soften the mechanical damage or splash that may occur to the bioink due to the fall, if the need for it arises.

CHAPTER IV

EXPERIMENTAL SETUP AND RESULTS

4.1 Chapter Overview

Chapter IV details the experimental setup used along with the results obtained from the experiment. Section 4.2 describes the laser micromachining portions of the experiment through the beam route used along with the primary software that controls the beam in 4.2.1, the software that controls the 3-axis stages and secondary beam functions is seen in 4.2.2, the system's etching capabilities on various substances are shown in 4.2.3, and a sample of the cutting capabilities in 4.2.3. Section 4.3 details the mixture used to coat the quartz in the ribbon for bioprinting. Section 4.4 explains the spin coating method used to determine the parameters to coat the quartz with the mixture at different thicknesses. Section 4.5 details the ribbon composition in full. Section 4.6 includes the design of the experiment being conducted along with the equipment being used to analyze the results. Section 4.7 shows the results of the experiment, section 4.7.1, as well as an analysis of said results, section 4.7.2.

4.2 Laser Micromachining

The modular laser system incorporates a near infrared femtosecond YAG laser manufactured by Spectra Physics that utilizes a 2 mm beam diameter. Through the use of secondary and auxiliary equipment, the beam diameter is altered to meet micromachining standards: machining in the micro level. Similar to traditional manufacturing processes, such as

turning and milling, laser machining is a type of subtractive manufacturing where material is taken away from a workpiece or starting material. When enough thermal energy from the laser is absorbed, the material undergoes heating, melting, and evaporation [21]. The result is a workpiece incorporating the desired geometry: shapes, pattern, and holes. In addition, Butkus et al. (2016) stated that femtosecond lasers are greatly compatible for micromachining purposes due to the high intensity achieved by the pulses once the laser beam is focused [22]. Several tests were carried out to determine the laser machining and micromachining capabilities of the system.

4.2.1 Beam Route

The system is dependent on the laser beam, controlled through the Spectra Physics software, for machining. Through this software the laser is turned on, put into standby, or turned off completely. The laser power, number of pulses, and the shutter can all be controlled through this interface, though power and pulse production can also be changed to external control so that another software can be in command of these parameters. The interface of the initial software can be observed in Figure 4.1.

Figure 4.1 Initial Software Interface

An important part of the experiment is determining if the beam follows the appropriate path and is adequately focused through the galvanometer. As previously mentioned, the upper half of the system encompasses the laser, a beam expander and a set of optical mirrors. A schematic of the desired beam route can be observed in Figure 4.2. Once the laser is activated, a beam is created and magnified through the expander, located a few inches from the laser opening. The expander enlarges the beam and is directed from the first 45-degree optical mirror the second mirror, orientated to move the beam downwards towards the optical mirror mounted on the galvanometer. This optical mirror is mounted at a 45-degree angle to orient the beam from the vertical direction to a horizontal one to be able to enter the side of the galvanometer. The laser is then focused, and the beam diameter enters the micro level 83.1mm after leaving the galvanometer towards the XY stage. To be able to adjust the Z-stage such that the object being worked on was 83.1mm from the galvanometer for optimal beam activity, gauge blocks were used to measure the distance from the lens attached on the galvanometer to the top of the XY stage. This measurement, of approximately 124.6886mm at a Z-stage position of Z = 148mm, was then used to determine the minimum height for the ribbon, or for any other object, needed to optimally work on it with the laser.

The near infrared laser, with a 1040 nm wavelength, restricts us in determining if the laser path is correct or followed. The visible spectrum, dictating the wavelengths able to be seen through the human eye, ranges from approximately 380 nm to 780 nm [23]. Initially, a laser pen was utilized, in place of the beam expander, to visibly determine that the setup was working. Once the optical and expander placement were confirmed, the Spectra Physics software was used to turn on the laser, set the power to roughly 20% max power, and set the number of pulses to around $1/10^{th}$ of the maximum pulses per second to generate a low energy level. Afterwards, a

near infrared sensor card, capable of confirming infrared wavelengths, was utilized at several locations to confirm the beam path.

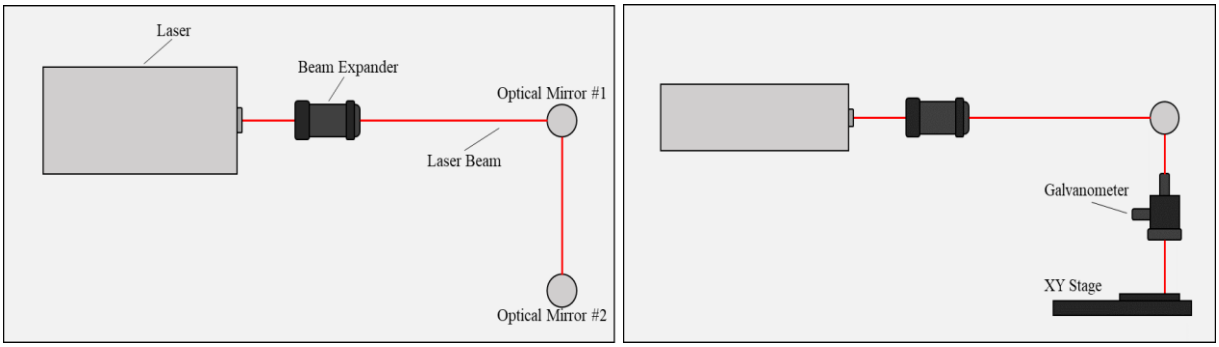

Figure 4.2 Beam Route Schematic

4.2.2 Aerotech Software

The Aerotech software is composed of multiple auxiliary software that helps control the laser system, the stages, and data capture of various parameters of the laser and stages. The A3200 Motion Composer software, whose interface can be seen in Figure 4.3, is the software used to create the code to control the XYZ stage positions and motions along with the power, pulses, and state of the laser along with several other capabilities.

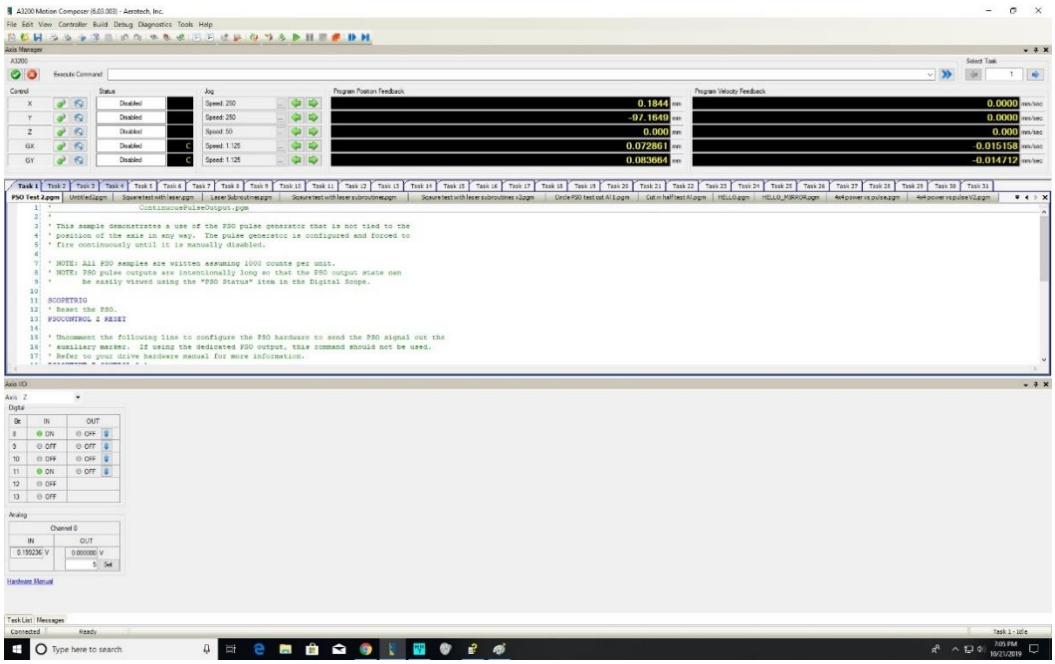

Figure 4.3 Software Interface

The software allows for the control of the position of the stages up to three or four decimal points in terms of millimeters and time wise has millisecond to microsecond capabilities, each depending on what parameter is being controlled. The coding is written using Aerotech's own language which mimics G or M coding while allowing for the use of either its own language or G/M coding.

4.2.3 Etching

Etching, a subset of laser marking and cutting, uses a high intensity laser beam to mark a pattern over a specified area with high precision and high accuracy, creating a depth of 2.54 micrometers or less [24]. Utilizing a femtosecond laser, with ultra-short pulsing characteristics, more meticulous features can be etched. With the Aerotech software, several etching attempts were carried out and can be observed in Figure 4.4. The left portion of the figure demonstrates a circle being formed on top of several aluminum sheets, the right portion shows several equally

distanced squares created on steel, and the bottom portion showcases several overlapping letters that spell the word “HELLO” on a different steel sheet. All three instances were running at max laser power controlled by the Aerotech software, but with differing feed rates and number of passes. The circle was created at the highest feed rate 40 mm/sec with the most number of passes, the “HELLO” was created at half the feed rate of the circle with 20mm/sec and only 1 pass, and the squares were made at the slowest feed rate of the three with only 1mm/sec and 5 passes each.

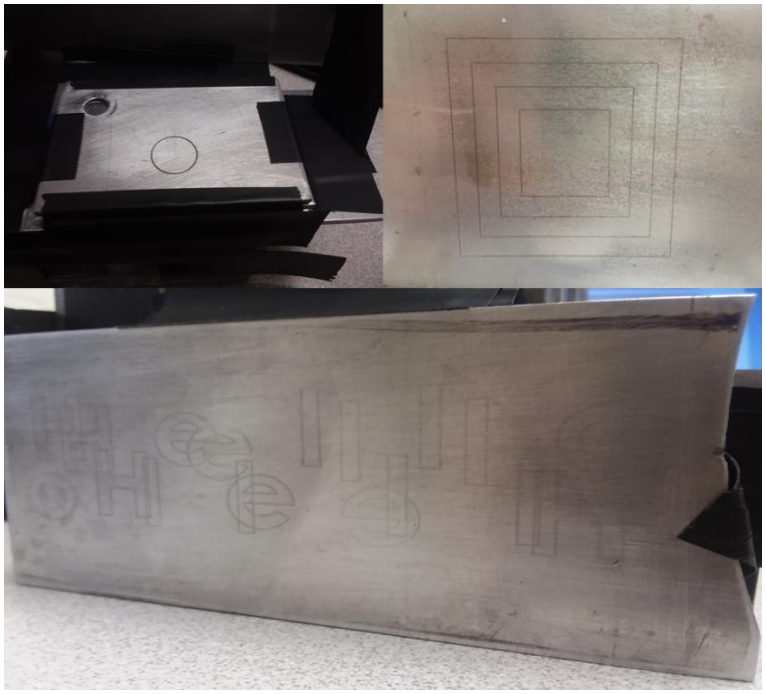

Figure 4.4 Etching Examples on Aluminum/Steel Sheets

Etching was also attempted on wood and acrylic, but due to the absence of a vacuum or fan to take care of the smoke that resulted from the laser and wood/acrylic interaction, it was deemed best to halt those exams to prevent the smoke from damaging the lens and personnel. This does not mean that the short preliminary tests failed, as the laser was able to produce markings on both materials.

4.2.3 Cutting

Aside from etching on steel and aluminum, tests were also run to cut thin lines on pieces of aluminum foil. Though the pieces of aluminum were not perfectly flat, the needed design was indeed cut into the foil. Figure 4.5 shows a microscopic view of one of the cuts created in a piece of aluminum foil with a width of approximately 125um.

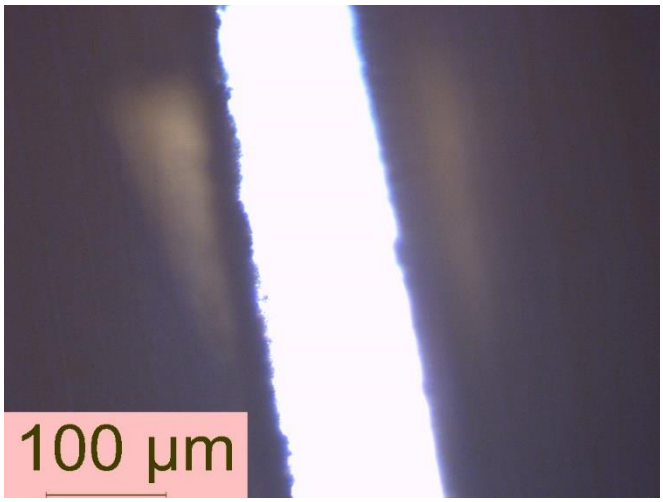

Figure 4.5 Zoomed in View of Cut on Aluminum Foil

4.3 Alginate Mixture

4.3.1 Alginate Properties

The material of interest for the bioprinting portion of the experiments are a distilled water and sodium alginate solution at varying percentages. Sodium alginate, in the form of odorless solid powder, was purchased from Thermo Fisher Scientific and is comprised of alginic acid and sodium salt molecules [25]. Alginates are polysaccharides, a type of hydrophilic carbohydrate incorporating several sugar molecules, found naturally in brown algae and accounts for over 35% of the entire weight once water is extracted [26]. Characteristics that enable alginates to be favored in bioprinting process include the material's low cost, biocompatibility, and ability to not

negatively interfere with biological systems [27]. Properties pertaining to the sodium alginate powder can be found in Table 4.1.

Table 4.1: Alginate Properties [25]

Property [unit]	Sodium Alginate
CAS-No	9005-38-3
Chemical Formula	C6H9NaO7
Components	Algenic acid, sodium salt
State	Powder Solid
Color	Dark Yellow
Melting Point [^{o}C]	> 300
ph*	5.5-7.5

* 1% aq. sol. (20^{o}C)

4.3.2 Sodium Alginate Solution

The sodium alginate and distilled water solutions were created by using a Ninja brand blender with four different solutes to solvent weight ratios, which can be observed in Table 4.2. The distilled water was kept constant at 100 ml and the sodium alginate was varied between 1g through 4g, at equally spaced intervals. A tare electronic scale and a glass beaker were used to measure and transport the materials into the blender. The distilled water was poured first into the blender, followed by the sodium alginate to prevent material sticking to the plastic walls. In addition, the sides of the blender container were scraped with a plastic spoon after the first minute of mixing. The lowest rotational speed was used for each weight ratio and the mixing time was set to 45 minutes. The process was carried under room temperature, 20^{o}C, and the beaker and blender were rinsed with distilled water and dried before usage to avoid contamination. Table 4.3 illustrates the density differences between the four solutions. They all seem to have roughly the same density, with an average of 1029.380 mg/mL and a standard

deviation of 14.55 mg/mL, which is only 1.41% of the average value. It was also noticed that the viscosity seemed to increase as the concentration of sodium alginate increased.

Table 4.2: Solution Percentages

Sodium Alginate	Distilled Water	Solution %
1g	100ml	1%
2g	100ml	2%
3g	100ml	3%
4g	100ml	4%

Table 4.3: Solution Density

Solution	Density (mg/um^3)	Density (mg/ml)
1%	9.896E-10	1010.499
2%	9.743E-10	1026.43
3%	9.650E-10	1036.313
4%	9.576E-10	1044.278

4.4 Spin Coating: Alginate Mixture

To find the parameters needed to obtain the thicknesses for each of the four sodium alginate solutions, systematic trial and error was conducted due to most of the literature revolving around depositing metals or drying out the liquid. A 1 mL syringe was used to withdraw and place 0.5 mL portions of the sodium alginate solution, which are dyed red for better visibility as opposed to the clear color it is naturally, from their containers (seen in Figure 4.6) to the top of a quartz disc after it was placed in the VTC-100 Vacuum Spin Coater from MIT Corporation (seen if Figure 4.7). The quartz disc was kept in place in a chuck on the spin coater by a vacuum created from the accompanying vacuum motor seen in Figure 4.7 while adhered to a piece of blue tape to reduce the chance of cracking the quartz. The settings were changed on the spin coater prior to turning on the vacuum as they cannot be changed while the

vacuum is on. Once the 0.5 mL solution was on the quartz, a pipette tip was used to carefully spread out the solution to evenly cover the entirety of the quartz before commencing spin coating.

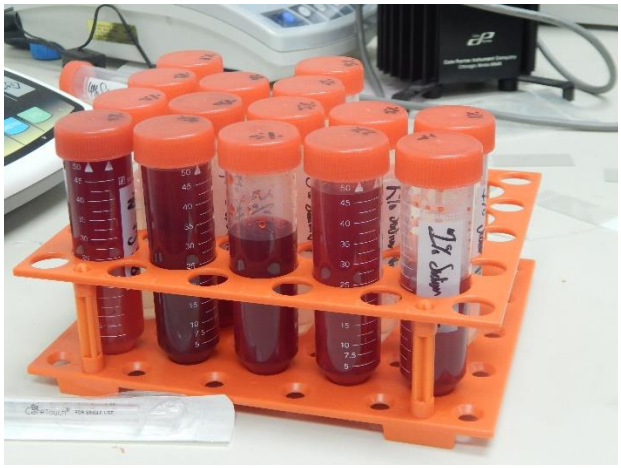

Figure 4.6 Sodium Alginate Solutions

Figure 4.7 Spin Coater

To find the thicknesses of the bioink layers, the relationship between mass, volume, and density was used, i.e. Density = Mass/Volume. The mass of the quartz was measured each time before spin coating using a high precision scale (seen in Figure 4.8) to ensure accuracy, as well

as after spin coating to determine the amount of mass added by the bioink. Using the relationship to density, the increase in mass was divided by the density to determine the volume of the bioink layer. Using the assumption that the spin coating left an evenly distributed layer over the area of the quartz, the obtained volume was divided by the surface area of the face of the quartz to obtain the thickness of the bioink layer. This was conducted multiple times for each concentration of sodium alginate until the four desired thicknesses were able to be achieved repeatedly. All the trials, calculations, and data were kept in an excel file on an excel file. A picture of a quartz disc with a spin coated layer of bioink can be seen in Figure 4.9.

Figure 4.8 High Precision Scale

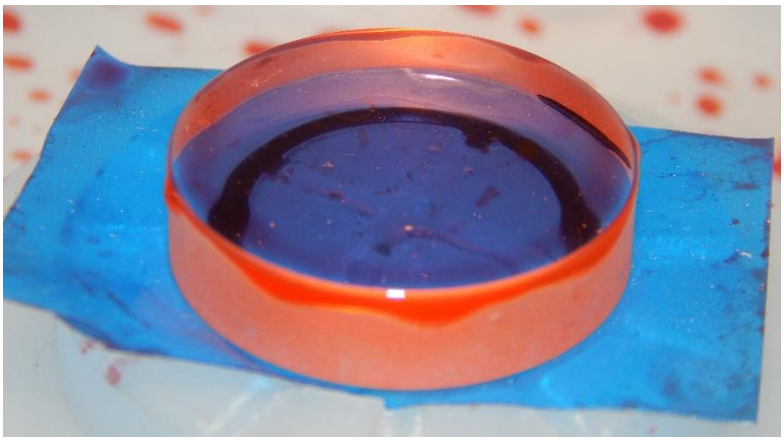

Figure 4.9 Quartz Disc with a Bioink Layer

4.5 Ribbon

The ribbon, which is used to hold to donor and receiving substrates made up of quartz discs, is comprised of two almost identical aluminum parts deemed substrate holders. The differences between the two substrate holders are the holes for the screws that connect them together as well as the bottom holder having a wider bottom portion to reinforce the base. In order to create a small separation between the two substrate holders to obtain a small working distance from the donor substrate to the receiving substrate, films of Kapton tape with a 50um thickness were placed on both sides of the top substrate holder. The number of films depended on the thickness of the bioink layer in order to keep the working distance almost the same throughout each thickness value. The donor and receiving quartz substrates themselves were held in place in the substrate holders by 4mm ball end screws through holes located on the sides of the substrate holders. Figure 4.10 shows the ribbon components in three different pictures while Figure 4.11 shows a close-up view of the separation between the donor and receiving substrates without a bioink layer. Picture (a) shows the receiving substrate portion already secured onto the

XY platform, picture (b) shows the donor substrate portion with Kapton films and a substrate without a bioink layers, and picture (c) shows the entire ribbon system.

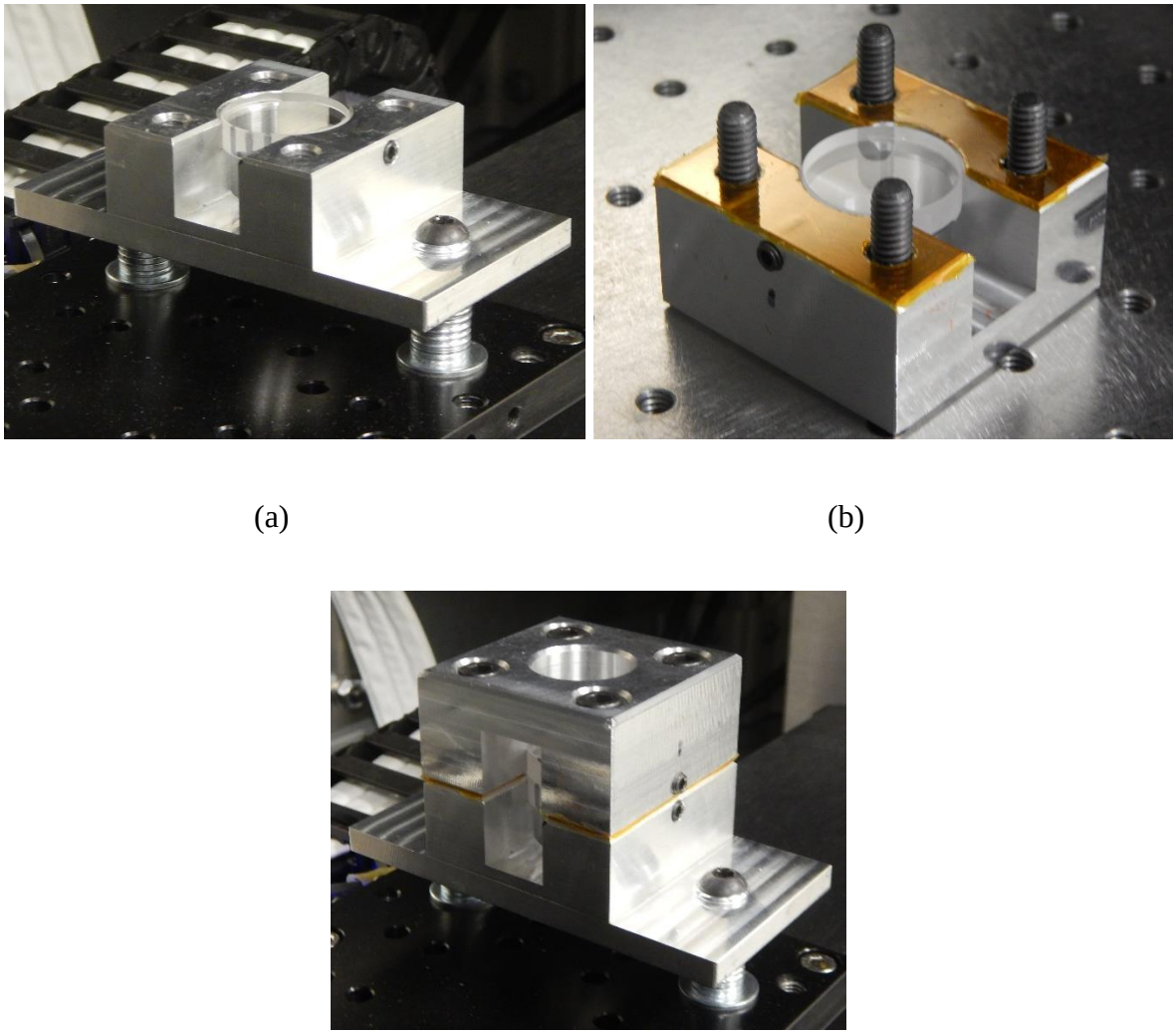

(a) (b)

(c)

Figure 4.10 Donor Substrate Section (a), Receiving Substrate Section (b), and Full Ribbon (c)

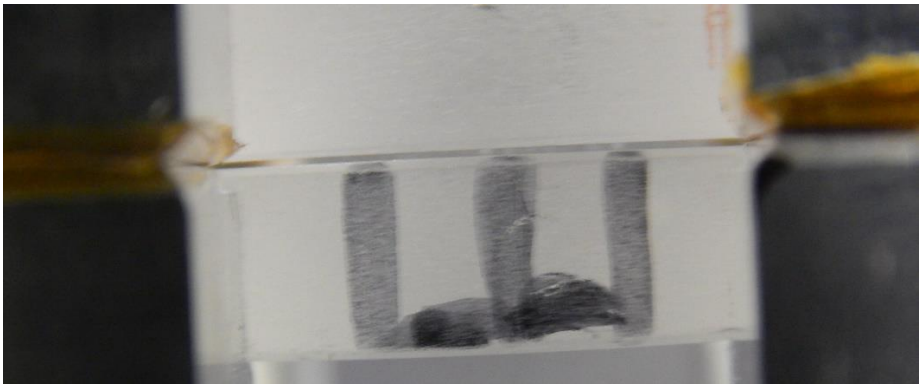

Figure 4.11 Separation Between Donor and Receiving Substrates without Bioink Layer

4.6 Design of Experiments

As previously stated, the design of experiments revolved around a four by four factorial design. The four factors in question are the laser power, the number of laser pulses, the concentration of the sodium alginate concentration, and the thickness of the bioink layer to be spin coated on the donor quartz substrate. The sodium alginate concentration factor can be broken up into density and viscosity to be able to have a relationship between these two sub factors and the droplet size, but the densities being used are within a 1% range and the viscosity will be left to be measured post experiments. Each of the four factors has four levels, or values, which is to be tested and used to analyze the effect of the factor with the size of droplets to determine the optimal condition(s), if any while using these values, to print bioink droplets with the laser. The four values of each factor can be seen in Table 4.4 below.

Table 4.4: Four Factors with Four Levels

Laser Power (V)	Laser Pulses	Concentration (%)	Bioink Thickness (um)
1.25	1	1%	35
2.5	2	2%	50
3.75	3	3%	75
5	4	4%	90

The original four levels for the laser pulse factor were 10, 100, 1000, and 10000, but due to reasons explained in section 4.7, the values were lowered to 1, 2, 3, and 4. To find the power of the laser in Watts as opposed to volts, which is how Aerotech controls the laser, the power was measured via the advanced screen in the Spectra Physics software which is initially used to control the laser. The power was set to the four different voltages seen in Table 4.4 through the Aerotech software, and then the power in watts was viewed in the Spectra Physics software screen seen in Figure 4.12 while the laser pulses were running at 200Khz. The laser power in watts can be seen in Table 4.5.

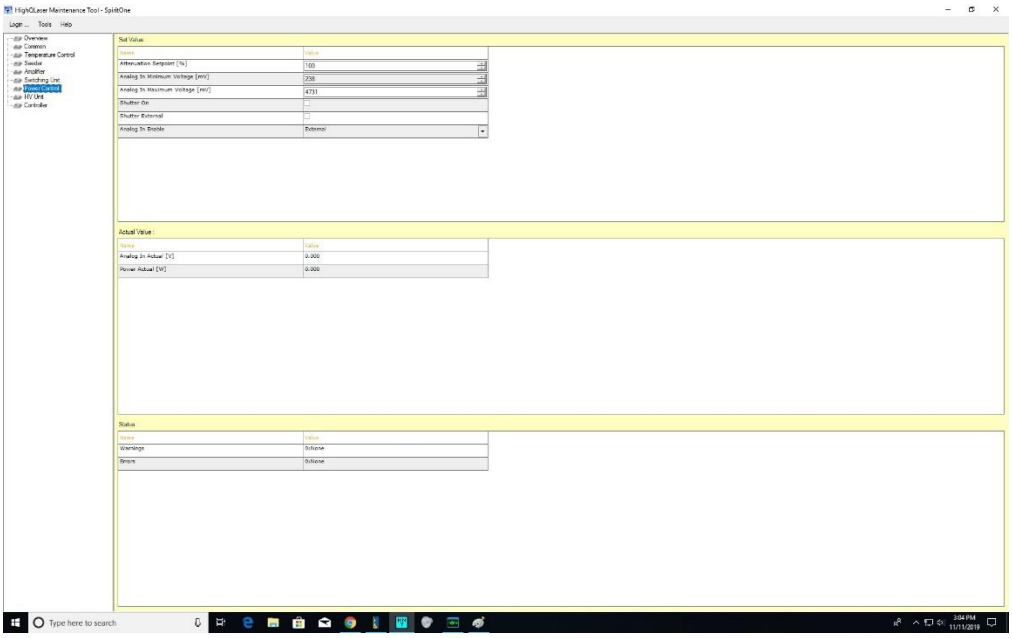

Figure 4.12 Spectra Physics Advanced Screen

Table 4.5: Laser Power in Watts

Laser Power (V)	Laser Power (W)
1.25	1.797
2.5	4.062
3.75	6.312
5	8.082

The fact that the design of the experiment is a four by four factorial means that there are 216 different combinations needed to be tested. In reality, only sixteen experiments were needed to obtain all 216 different combinations since each experiment used one bioink thickness, one sodium alginate solution concentration, and one four by four laser firing array of laser power versus laser pulses. Essentially each of the sixteen combinations created by the four levels from the solution concentration and the bioink thickness was used only once in combination with the four by four array of laser firing sequences that varied in laser power and pulses. This laser firing sequence array can be seen in Figure 4.13. Each dot represents one of the 16 different power to pulse combinations and is separated from the other dots by 150 micrometers in the X and Y directions. The black dot represents the center of the quartz substrate in the ribbon with respect to the galvanometer.

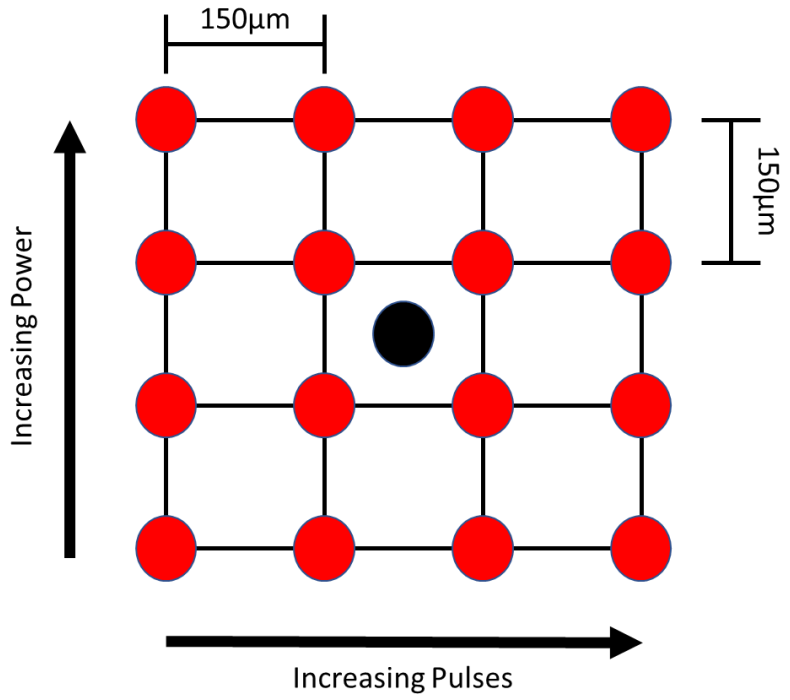

Figure 4.13 Laser Firing Sequence Array, Laser Power Vs. Laser Pulses

In order to obtain the response variably of droplet size, an optical microscope (seen in Figure 4.14) was used at varying magnifications.

Figure 4.14 Optical Microscope

4.7 Results and Analysis

The results of a preliminary test using 3% sodium alginate solution at 35um at the four laser power levels and the original laser pulse levels of 10, 100, 1000, and 10000 can be seen below in Figure 4.15 in two magnifications. The picture shows multiple light up circular holes. The reason there is more than one set of four by four array of sixteen holes is because they test was conducted multiple times at slightly different laser to ribbon working distance to understand if that factor was the cause for the holes. The holes that can be seen in Figure 4.15 signify that the laser, at these settings and pulse amounts, actually “drilled” into the receiving quartz disc. It can be ensured that the holes are actually holes and not droplets since after wiping and cleaning

down the quartz, the holes were still there each and every time. The deepness of the holes was measured and found to be between 50 to 90 microns deep.

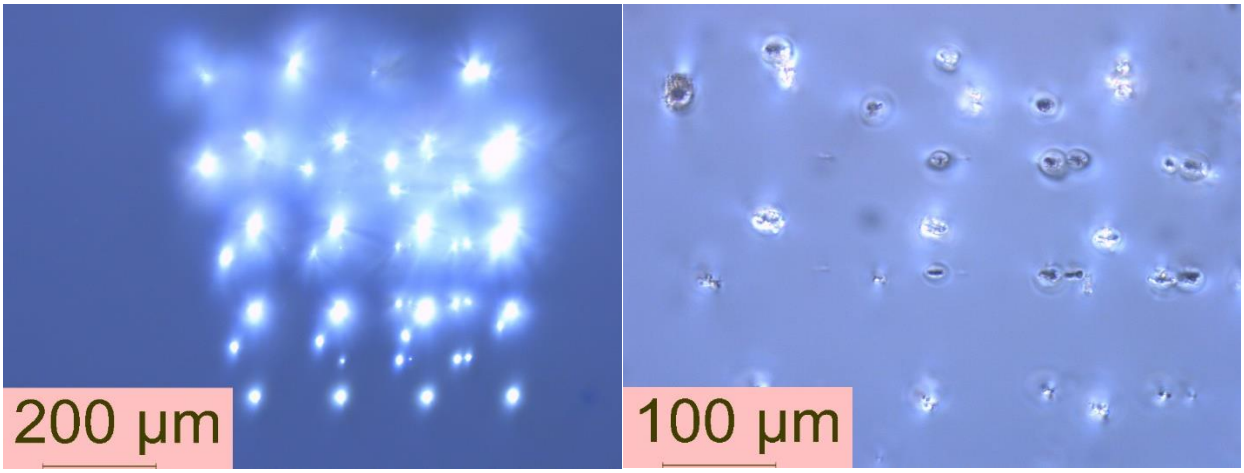

Figure 4.15 Magnification of Holes Created with the Original Number of Laser Pulses

Since even the lowest number of pulses, 10, was able to create a defect in the receiving quartz, the number of pulses was lowered to 1, 2, 3, and 4 in the hopes that they would provide better results. After conducting all sixteen experiments that encompass all 216 combinations in the four by four factorial with the lowered laser pulse levels, no droplets could be seen through the optical microscope. The list of the sixteen combinations, along with the spin coating parameters, and whether the experiment was completed and formed droplets or not can be seen in Table 4.6.

Table 4.6: Experimental Results

Bioink thickness	Sodium Alginate %	t1	RPM1	t2	RPM2	Experiment Completed? Y/N	Droplets? Y/N
35	1	30	500	5	2000	Y	N
	2	30	600	30	2200	Y	N
	3	30	1000	25	3500	Y	N
	4	30	1000	30	3500	Y	N
50	1	25	500	10	1200	Y	N
	2	30	600	15	2200	Y	N
	3	30	600	40	2500	Y	N
	4	30	600	40	2500	Y	N
75	1	15	600	5	1000	Y	N
	2	30	600	5	2200	Y	N
	3	30	600	30	2200	Y	N
	4	30	600	36	2100	Y	N
90	1	15	500	5	1000	Y	N
	2	30	500	5	2000	Y	N
	3	30	600	25	2000	Y	N
	4	30	600	20	2100	Y	N

There are many reasons as to why no droplets could be seen from any of the experiments conducted with these value parameters. For starters, the process was not undergone in a controlled environment. This means that the humidity, dust, temperature, air flow, and many other environmental factors were not controlled that could have affected how fast the droplets, if any, dried up from when the experiment was started, to when the quartz was underneath a microscope. It could also be possible that there were droplets on the quartz, but the dye used on the solution thinned out too much during spin coating that the small droplets could not be differentiated through the microscope, especially if there were not more than two or three to stand out in a man-made pattern. The energy created by the power and pulse number combination could also just have been too much to effectively create a droplet under the circumstances even though they did not create any defects in the receiving quartz unlike the

original pulse values. The spin coating layer could have been an issue if it was not perfectly spread out.

It could be that a titanium layer, or other sacrificial layer, should have been used in order to create droplets. If the laser could have caused a hole in the titanium in such a manner that the heat interaction between the laser, titanium, and bioink layer formed a bubble, then it is possible droplets would have been seen. The thickness of the donor quartz could have also been an issue considering the many possible interaction the laser could have had with it due to its size, alignment, or any imperfections on the surface. At one point, it was an option that maybe the software could not make the laser fire between one to four pulses, but after using Aerotech's scope trig software to data capture firing sequences throughout the code, the pulse firing events could be seen in a plot which is shown in Figure 4.16. The possibility that the experiments resulted in droplet formations is also feasible, and if the area of interaction was being viewed under a camera, then maybe it would've verified the presence, or absence, of droplets.

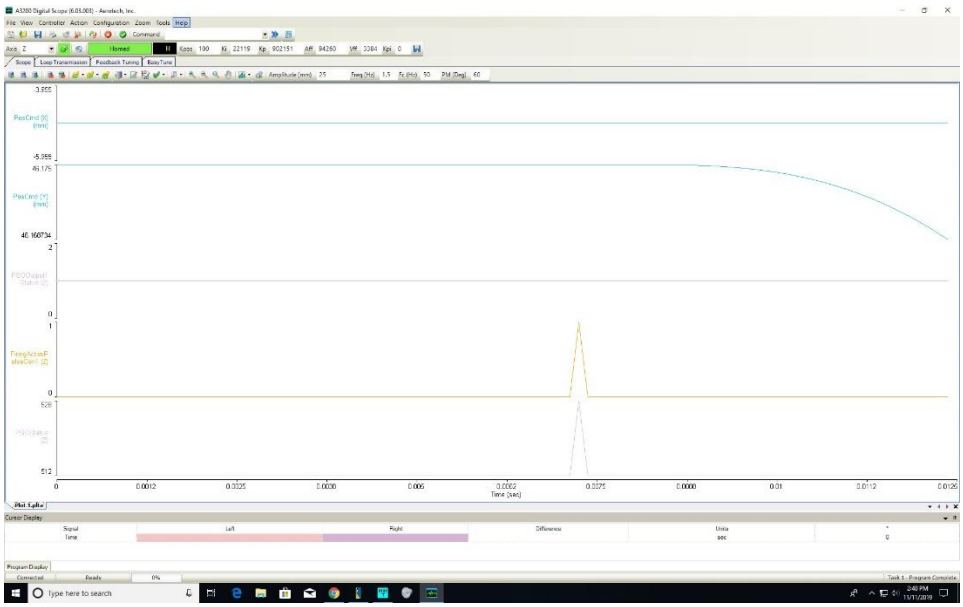

Figure 4.16 Pulse Firing Event Data Capture

One major reason as to why the experiment may not have been successful lies in the laser fluences, or energy densities, used in the experiment. It is reasonable to assume that the laser fluence was too high of an energy density for the biomaterial to handle and simply vaporized the bioink portion exposed to the laser pulses. Combining the high fluence used with the extremely short distribution time of a few microseconds could also have been a factor due to the sudden transfer of relatively high energy in a small area in an ultrashort timespan. Considering an average spot size of 20 microns, the laser fluences formed by using the 4x4 power to pulse parameter array can be seen in Table 4.7. Considering Zhang, Z. et al were able to produce and view various jetting occurrences while performing a similar experiment using sodium alginate solutions and fluences ranging from 500-2900 mJ/cm^2 [28], it would make sense if the power and pulse combinations with laser fluences in Table 4.7 that are within that range to have produced some form of jet or droplet. At the same time, the statement can't be said with one hundred percent confidence since the two laser wavelengths and pulse durations used in both experiments are vastly different. The laser used here has a wavelength and pulse duration of 1040nm and <400fs respectively, while Zhang, Z. et all used a 193nm laser with 12ns pulse duration. This longer pulse duration means that the laser fluence was distributed more slowly, which could have played a factor into why the experiment conducted here may have not produced any droplets. Therefor, laser fluence may have to be turned down to a lower energy density in order for this setup to produce droplets.

Table 4.7: Laser Fluences Created by the 4x4 Power to Pulse Array

Accumulated Pulse Fluence (mJ/cm^2)		Laser Pulses			
		1	2	3	4
Pulse Fluence (uj/um^2)	0.032157	3215.726	6431.451	9647.177	12862.9
	0.025115	2511.465	5022.93	7534.395	10045.86
	0.016162	1616.218	3232.437	4848.655	6464.874
	0.00715	715.0036	1430.007	2145.011	2860.014

In the end, the results were inconclusive as to whether these specific parameter values could, or could not, result in bioink droplets for the reasons mentioned above. It is inconclusive since it is possible that droplets were formed, but due to the environmental conditions and the lack of surveillance at the laser and bioink interface, it was not apparent if they were. Even though it is true that these experiments could be valid, that the values could not create droplets, that a sacrificial titanium layer might be needed, and that laser fluence may need to be lowered, the fact remains that the results could be different in a controlled environment and/or if they were viewed at the interaction interphase.

CHAPTER V

CONCLUSION

5.1 Chapter Overview

Chapter 5 concludes the study with a review and summary of the capabilities of the laser system and results in section 5.2. It also illustrates future work to be done with the project in section 5.3.

5.2 Results

The modular laser system was found to be stable and useful in multiple micromachining application. It was proven to be able to etch complex figures in both aluminum and steel, along with promising etching abilities with wood and acrylic given some safety modification. The system could also create thin slices in aluminum foil. As for the bioprinting capability experiment, though the results show a failure to produce droplets under these parameter values and causing holes in the quartz with the original values, it is still inconclusive as to whether droplets were formed or not for the reasons stated in section 4.7. It could be that droplets were formed but were dried out and essentially unable to be found under the optical microscope. Regardless, studies have proven that bioprinting via laser induced forward transfer is possible, and with some slight modification to the experiment, environment, and observation methods, this modular laser system should be capable of the same.

5.3 Future Work

There is much to do when it comes to future work involving the laser system designed and built here. A controlled environment needs to be set up, preferably one where humidity, air temperature, air flow and such are controlled. Even if it is a simple controlled environment that surround the area around the ribbon and motion stages, it would help the project move along. If possible, a positive pressure environment to keep the dust and contaminates out of the experimental area would be preferable, especially once cells are introduced. A vacuum or air flow system would also be effective, especially when dealing with work on solids such as metals, woods, and plastics due the smoke that arises from the laser interaction. If a simple vacuum system is placed, etching testing should be able to be conducted on wood and plastics without having to worry about the relatively heavy number of fumes caused by the interactions. At the same time, laser testing, like etching, can be done on titanium plates to understand the interactions the system has with titanium. In terms of titanium, efforts should also be made to coating the quartz with a thin layer of titanium to conduct bioprinting experiments with a sacrificial layer. It may be beneficial as well to obtain a thinner quartz to reduce the distance the laser travels through the optical material.

The experiment should be conducted again with similar, or different, values but this time with a camera to see the droplet. Reproducing the experiment but with lower fluence values would also have to occur. The bioink could also be changed to include a collagen component since a different bioink with more substance could be more effective than simply a water and sodium alginate solution. If possible and the resources are there, inked cells should be mixed in with the solution to be able to better identify the droplets in case the solution dries out. In summary, there are many things that can and should be done for future work on the laser system

to be able to more effectively conduct bioprinting experiments as well as taking advantage of the systems other capabilities.

REFERENCES

[1] (n.d.). Retrieved from https://lasers.llnl.gov/education/how_lasers_work

[2] Svelto, O., & Hanna, D. C. (2010). *Principles of lasers*. Springer.

[3] Hildebrand, J., Hecht, K., Bliedtner, J., & Müller, H. (2011). Laser Beam Polishing of Quartz Glass Surfaces. *Physics Procedia, 12*, 452-461. Retrieved from https://www-sciencedirect-com.ezhost.utrgv.edu/science/article/pii/S1875389211001350.

[4] Ali, M., & Hung, W. (2017). 1.11 Micromachining. *Comprehensive Materials Finishing*, 322-343. Retrieved from https://www-sciencedirect-com.ezhost.utrgv.edu/science/article/pii/B9780128035818091566.

[5] Prakash, S., & Kumar, S. (2017). Microchannel fabrication via direct laser writing. *Microfabrication and Precision Engineering*, 163-187. Retrieved from https://www-sciencedirect-com.ezhost.utrgv.edu/science/article/pii/B9780857094858000061.

[6] Kaneda, Y. (2018). UV Lasers. *Encyclopedia of Modern Optics*, 446-450. Retrieved from https://www-sciencedirect-com.ezhost.utrgv.edu/science/article/pii/B978012803581809370X.

[7] Karazi, S., Ahad, I., & Benyounis, K. (2017). Laser Micromachining for Transparent Materials. *Reference Module in Materials Science and Materials Engineering*. doi:10.1016/b978-0-12-803581-8.04149-7

[8] Mishra, S., & Yadava, V. (2015). Laser Beam MicroMachining (LBMM) – A review. *Optics and Lasers in Engineering, 73,* 89-122. doi:10.1016/j.optlaseng.2015.03.017

[9] Zehra, K., Bashir, S., Hassan, S. A., Hayat, A., & Akram, M. (2018). Spectroscopic and morphological investigation of laser ablated silicon at various laser fluences. *Optik, 164,* 186-200. Retrieved from https://www-sciencedirect-com.ezhost.utrgv.edu/science/article/pii/S0030402618303413.

[10] Hospodiuk, M., Dey, M., Sosnoski, D., & Ozbolat, I. T. (2017). The bioink: A comprehensive review on bioprintable materials. *Biotechnology Advances, 35*(2), 217-239. Retrieved from https://www.sciencedirect.com/science/article/pii/S0734975016301719.

[11] Gao, Q., Zhao, H., Yang, F., Fu, J., & He, Y. (2018). Practical laboratory methods for 3D bioprinting. *3D Bioprinting for Reconstructive Surgery,* 7-32. doi:10.1016/b978-0-08-101103-4.00003-x

[12] Guillemot, F., Souquet, A., Catros, S., Guillotin, B., Lopez, J., Faucon, M., . . . Amédée, J. (2010). High-throughput laser printing of cells and biomaterials for tissue engineering. *Acta Biomaterialia, 6*(7), 2494-2500. doi:10.1016/j.actbio.2009.09.029

[13] Deng, Y., Renaud, P., Guo, Z., Huang, Z., & Chen, Y. (2017). Single cell isolation process with laser induced forward transfer. *Journal of Biological Engineering, 11*(1). doi:10.1186/s13036-016-0045-0

[14] Datta, P., Barui, A., Wu, Y., Ozbolat, V., Moncal, K. K., & Ozbolat, I. T. (2018). Essential steps in bioprinting: From pre- to post-bioprinting. *Biotechnology Advances, 36*(5), 1481-1504. doi:10.1016/j.biotechadv.2018.06.003

[15] Sklare, S., Phamduy, T. B., Curly, J. L., Huang, Y., & Chrisey, D. B. (2015). The Power of CAD/CAM Laser Bioprinting at the Single-Cell Level: Evolution of Printing. *3D Bioprinting and Nanotechnology in Tissue Engineering and Regenerative Medicine*, 79-103. doi:10.1016/b978-0-12-800547-7.00004-7

[16] Delaporte, P., & Alloncle, A. (2016). [INVITED] Laser-induced forward transfer: A high resolution additive manufacturing technology. *Optics & Laser Technology*, *78*, 33-41. doi:10.1016/j.optlastec.2015.09.022

[17] Zhang, Z., Xu, C., Xiong, R., Chrisey, D. B., & Huang, Y. (2017). Effects of living cells on the bioink printability during laser printing. *Biomicrofluidics, 11*(3), 034120. doi:10.1063/1.4985652

[18] Duocastella, M., Colina, M., Fernández-Pradas, J., Serra, P., & Morenza, J. (2007). Study of the laser-induced forward transfer of liquids for laser bioprinting. *Applied Surface Science*, *253*(19), 7855-7859. doi:10.1016/j.apsusc.2007.02.097

[19] Zaharieva, J., Milanova, M. (2017). Thin Films immobilization of Complexes with Optical Properties. *Intech Open*. 251- 270

[20] Yusuf, Y., Azis, R.S., Mustaffa, M.S. (2018). Spin-Coating Technique for Fabricating Nickel Zinc Nanoferrite (Ni0.3Zn0.7Fe2O4) Thin Films. *Intech Open*. 259 – 273

[21] Dubey, A.K., Yadava, V. (2008). Laser beam machining – A review. *International Journal of Machine Tools & Manufacture 48*. 609-628

[22] Butkus, S., Alesenkov, A., Paipulas, D., Baipulas, T., Kaskelyte, D., Barjuaskas, M., Sirutkaitis, V. (2016). Micromachining of Transparent, Semiconducting and Metallic

Substrates Using Femtosecond Laser Beams. *Journal of Laser Micro/Nanoengineering 11*. 81 – 85

[23] Basic UV-Vis Theory, Concepts and Applications. *Thermo Spectronic*. 1-28

[24] What is Laser Etching & Engraving? (2019). *MECCO*. Retrieved from https://www.mecco.com/application-laser-etching-engraving

[25] Safety Data Sheet (2018). *Thermo Fisher Scientific*. 1 – 6

[26] Aprilliza., H., Aprilliza, M. (2017). Characterization and properties of sodium alginate from brown algae used as an ecofriendly superabsorbent. *Materials Science and Engineering 188*.

[27] Lee., K.Y, Mooney, D.J. (2012). Alginate: properties and biomedical applications. *Prog Polym Science 37*. 106-126

[28] Zhang, Zhengyi, et al. "Time-Resolved Imaging Study of Jetting Dynamics during Laser Printing of Viscoelastic Alginate Solutions." *Langmuir*, vol. 31, no. 23, Apr. 2015, pp. 6447–6456., doi:10.1021/acs.langmuir.5b00919.

[29] M. Colina, P. Serra, J.M. Fernández-Pradas, L. Sevilla, J.L. Morenza, "DNA deposition through laser induced forward transfer", *Biosensors and Bioelectronics*, Vol 20, Issue 8, 2005, pp. 1638-1642, ISSN 0956-5663, https://doi.org/10.1016/j.bios.2004.08.047.

[30] A. Karaiskou, I. Zergioti, C. Fotakis, M. Kapsetaki, D. Kafetzopoulos, "Microfabrication of biomaterials by the sub-ps laser-induced forward transfer process", *Applied Surface Science*, Volumes 208–209, 2003, pp. 245-249, ISSN 0169-4332, https://doi.org/10.1016/S0169-4332(02)01396-X

[31] *Spirit. High Repetition Rate, High Average Power Ultrafast Laser.* SP-DS-20170823. Spectra-Physics. 2017

[32] *S6EXP0050/328 Beamexpander.* Issue A. Sill Optics. July 2017

[33] *Aerotech*, https://www.aerotech.com/product-catalog/laser-scan-heads/nmark-agv-hp(o).aspx?search-auto-complete=true.

[34] *Integrity 3 VCS 4.8 Mm Skin Optical Tables with One Tuned Damper and Pneumatic Isolation*, https://www.newport.com/f/integrity-3-vcs-table-systems-with-1-tunable-damper?q=integrity 3:relevance:isObsolete:false.

APPENDIX

APPENDIX

CODE FOR EXPERIMENTS

Aerotech Code for Etching Circle in Aluminum

```
DVAR $MVAR $ZVAR

ENABLE X Y

‘SCOPETRIG

ABLSOLUTE

F 40

CALL LaserPower p0 ‘Make sure Laser power is 0

CALL LaserPower p5 ‘Laser power at a certain voltage

‘Setup Laser

PSOCONTROL Z RESET

PSOOUTPUT Z CONTROL 0 1

$ZVAR = 127.

LINEAR

LINEAR X -30 Y 60
```

```
CALL LaserOn

dwell .5

WHILE $ZVAR < 130

        REPEAT 5

                CW X -30 Y 60 I -5 J 0

        ENDREPEAT

        $ZVAR = $ZVAR + .01

        LINEAR Z $ZVAR

ENDWHILE

CALL LaserOff

CALL LaserPower P0

END PROGRAM

'''

DFS LaserOn

        PSOCONTROL Z ON

ENDDFS

DFS LaserOff

        PSOCONTROL Z OFF
```

```
ENDDFS

DFS LaserPower

        $AO[0].Z = $p

ENDDFS
```

Aerotech Code for Etching Multiple Squares in Steel

```
DVAR $MVAR $RX $LX $UY $LY $THICKNESS

ENABLE X Y

'HOME X Y

ABSOLUTE

F 1 'Define Speed of Axis movement

CALL LaserPower p0 'Make sure Laser power is 0

CALL LaserPower p5 'Laser Power at a certain voltage

'Setup Laser

PSOCONTROL Z RESET

PSOOUTPUT Z CONTROL 0 1

'initial square corner coordinates

$RX = -55 'right x side

$LX = -5 'left x side
```

```
$UY = 25 'upper y side

$LY = 75 'lower y side

$THICKNESS = 5 'set the amount of spacing between squares

"'laser on, movement, laser off loops

" first loop

G1 X $RX Y $LY 'Go to lower right edge of square start point

'CALL LaserOn 'Laser on

PSOCONTROL Z ON

'Square loop with x number of passes

FOR $MVAR = 0 TO 4

G1 X $LX Y $LY 'lower left point

G1 X $LX Y $UY 'upper left point

G1 X $RX Y $UY 'upper right point

G1 X $RX Y $LY 'lower right point (startpoint)

NEXT $MVAR

'End square loop

'Laser Off

Call LaserOff
```

```
" second loop

$RX = $RX + $THICKNESS 'adjust right x side

$LX = $LX - $THICKNESS 'adjust left x side

$UY = $UY + $THICKNESS 'adjust upper y side

$LY = $LY - $THICKNESS 'adjust lower y side

G1 X $RX Y $LY 'Go to lower right edge of square start point

'CALL LaserOn 'Laser on

PSOCONTROL Z ON

'Square loop with x number of passes

FOR $MVAR = 0 TO 4

G1 X $LX Y $LY 'lower left point

G1 X $LX Y $UY 'upper left point

G1 X $RX Y $UY 'upper right point

G1 X $RX Y $LY 'lower right point (startpoint)

NEXT $MVAR

'End square loop

'Laser Off

Call LaserOff
```

```
" third loop

$RX = $RX + $THICKNESS  'adjust right x side

$LX = $LX - $THICKNESS  'adjust left x side

$UY = $UY + $THICKNESS  'adjust upper y side

$LY = $LY - $THICKNESS  'adjust lower y side

G1 X $RX Y $LY 'Go to lower right edge of square start point

'CALL LaserOn 'Laser on

PSOCONTROL Z ON

'Square loop with x number of passes

FOR $MVAR = 0 TO 4

G1 X $LX Y $LY 'lower left point

G1 X $LX Y $UY 'upper left point

G1 X $RX Y $UY 'upper right point

G1 X $RX Y $LY 'lower right point (startpoint)

NEXT $MVAR

'End square loop

'Laser Off

Call LaserOff
```

```
''' fourth loop

$RX = $RX + $THICKNESS  'adjust right x side

$LX = $LX - $THICKNESS  'adjust left x side

$UY = $UY + $THICKNESS  'adjust upper y side

$LY = $LY - $THICKNESS  'adjust lower y side

G1 X $RX Y $LY 'Go to lower right edge of square start point

'CALL LaserOn 'Laser on

PSOCONTROL Z ON

'Square loop with x number of passes

FOR $MVAR = 0 TO 4

G1 X $LX Y $LY 'lower left point

G1 X $LX Y $UY 'upper left point

G1 X $RX Y $UY 'upper right point

G1 X $RX Y $LY 'lower right point (startpoint)

NEXT $MVAR

'End square loop

'Laser Off

Call LaserOff
```

```
'"End of laser square making loops

Call LaserPower p0 'Make sure Laser power is 0

End Program

'" subroutines

'DFS LaserOn

'       PSOCONTROL Z FIRE CONTINUOUS

'ENDDFS

DFS LaserOff

        PSOCONTROL Z OFF

ENDDFS

DFS LaserPower

        $AO[0].Z = $p

ENDDFS
```

Aerotech Code for Bioprinting Experiment

```
DVAR $CX $CY $dt1 $dt2 $dt3 $dt4 $dwelltime $to1 $to2 $to3 $to4 $kxk

ENABLE X Y Z

'HOME X Y Z

'SCOPETRIG
```

ABSOLUTE

F 10

'Setup Laser

PSOCONTROL Z RESET

PSOOUTPUT Z CONTROL 0 1

'Set the starting Z value such that working distance to the 'bottom' surface of the coated ribbon is 83.1

'LINEAR Z 145

'LINEAR Z 142.7886 (with 4 washers and 3 hex nuts)

'LINEAR Z 144.9886 '(with 12 washers up to the top of the bottom substrate)

LINEAR Z 144.8386 '(w/ 12 washers to the 'top' of the bioink)(for 35um and 50um)(original)

'LINEAR Z 144.7886 '(w.12 washers to the 'top' of the bioink)(for 75um and 90um)

'LINEAR Z 144.7386 '(w/ 12 washer to the 'top' of the bioink)(for 35um to 50um)(testing)(FAILED)

'"LINEAR Z 144.6886 '(w/ 12 washer to the 'top' of the bioink)(for 35um to 50um)(testing 2)

'LINEAR Z 144.6386 '(w/ 12 washer to the 'top' of the bioink)(for 35um to 50um)(testing 3)

'LINEAR Z 144.5886 '(w/ 12 washer to the 'top' of the bioink)(for 35um to 50um)(testing 4)

'LINEAR Z 144.5386 '(w/ 12 washer to the 'top' of the bioink)(for 35um to 50um)(testing 5)

'Ensure that the laser is currently at power level of zero (p ranges from 0 to 5 as Volts)

```
CALL LASERPOWER p0

'Set center point value

$CX = -4.73

$CY = 46.4

'set dwell time

$dt1 = .000005*2

$dt2 = .00001*2

$dt3 = .000015*1

$dt4 = .00002*1

$dwelltime = 2

'Set total time on in us (.1 sec = 100000 us)

$to1 = 5 '.000005 sec = 1 pulses

$to2 = 10 '.00001 sec = 2 pulses

$to3 = 15 '.000015 sec = 3 pulses

$to4 = 20 '.00002 sec = 4 pulses

'Go to center point

LINEAR X $CX Y $CY

F .1
```

```
SCOPETRIG

"" ROW 1

"'Code for coordinate 1:1

'Go to coordinate 1:1

LINEAR X $CX+.225 Y $CY+.225

'Set the power for the laser

CALL LASERPOWER p1.25

DWELL $dwelltime +.5

SCOPETRIG

'Set number of pulses and fire the laser

CALL LASERON t $to1 o $to1 k=1 d $dt1

'Set laser off

CALL LASEROFF

'"

"'Code for coordinate 1:2

'Go to coordinate 1:2

LINEAR X $CX+.075 Y $CY+.225

'Set the power for the laser
```

```
CALL LASERPOWER p1.25

DWELL $dwelltime +.5

SCOPETRIG

'Set number of pulses and fire the laser

CALL LASERON t($to2) o($to2) k=2 d($dt2)

'Set laser off

CALL LASEROFF

'''

'''Code for coordinate 1:3

'Go to coordinate 1:3

LINEAR X $CX-.075 Y $CY+.225

'Set the power for the laser

CALL LASERPOWER p1.25

DWELL $dwelltime +.5

SCOPETRIG

'Set number of pulses and fire the laser

CALL LASERON t($to3) o($to3) k=3 d($dt3)

'Set laser off
```

```
CALL LASEROFF

'''

'''Code for coordinate 1:4

'Go to coordinate 1:4

LINEAR X $CX-.225 Y $CY+.225

'Set the power for the laser

CALL LASERPOWER p1.25

DWELL $dwelltime +.5

SCOPETRIG

'Set number of pulses and fire the laser

CALL LASERON t($to4) o($to4) k=4 d($dt4)

'Set laser off

CALL LASEROFF

''''''''''''''''

'''' ROW 2

'''Code for coordinate 2:1

'Go to coordinate 2:1

LINEAR X $CX+.225 Y $CY+.075
```

```
'Set the power for the laser

CALL LASERPOWER p2.5

DWELL $dwelltime +.5

'Set number of pulses and fire the laser

CALL LASERON t($to1) o($to1) k=1 d($dt1)

'Set laser off

CALL LASEROFF

'''

'''Code for coordinate 2:2

'Go to coordinate 2:2

LINEAR X $CX+.075 Y $CY+.075

'Set the power for the laser

CALL LASERPOWER p2.5

DWELL $dwelltime +.5

'Set number of pulses and fire the laser

CALL LASERON t($to2) o($to2) k=2 d($dt2)

'Set laser off

CALL LASEROFF
```

'''

'''Code for coordinate 2:3

'Go to coordinate 2:3

LINEAR X $CX-.075 Y $CY+.075

'Set the power for the laser

CALL LASERPOWER p2.5

DWELL $dwelltime +.5

'Set number of pulses and fire the laser

CALL LASERON t($to3) o($to3) k=3 d($dt3)

'Set laser off

CALL LASEROFF

'''

'''Code for coordinate 2:4

'Go to coordinate 2:4

LINEAR X $CX-.225 Y $CY+.075

'Set the power for the laser

CALL LASERPOWER p2.5

DWELL $dwelltime +.5

'Set number of pulses and fire the laser

CALL LASERON t($to4) o($to4) k=4 d($dt4)

'Set laser off

CALL LASEROFF

""""""""""""""

"" ROW 3

"'Code for coordinate 3:1

'Go to coordinate 3:1

LINEAR X $CX+.225 Y $CY-.075

'Set the power for the laser

CALL LASERPOWER p3.75

DWELL $dwelltime +.5

'Set number of pulses and fire the laser

CALL LASERON t($to1) o($to1) k=1 d($dt1)

'Set laser off

CALL LASEROFF

"'

"'Code for coordinate 3:2

```
'Go to coordinate 3:2

LINEAR X $CX+.075 Y $CY-.075

'Set the power for the laser

CALL LASERPOWER p3.75

DWELL $dwelltime +.5

'Set number of pulses and fire the laser

CALL LASERON t($to2) o($to2) k=2 d($dt2)

'Set laser off

CALL LASEROFF

'''

'''Code for coordinate 3:3

'Go to coordinate 3:3

LINEAR X $CX-.075 Y $CY-.075

'Set the power for the laser

CALL LASERPOWER p3.75

DWELL $dwelltime +.5

'Set number of pulses and fire the laser

CALL LASERON t($to3) o($to3) k=3 d($dt3)
```

```
'Set laser off

CALL LASEROFF

'''

'''Code for coordinate 3:4

'Go to coordinate 3:4

LINEAR X $CX-.225 Y $CY-.075

'Set the power for the laser

CALL LASERPOWER p3.75

DWELL $dwelltime +.5

'Set number of pulses and fire the laser

CALL LASERON t($to4) o($to4) k=4 d($dt4)

'Set laser off

CALL LASEROFF

'''''''''''''''

'''' ROW 4

'''Code for coordinate 4:1

'Go to coordinate 4:1

LINEAR X $CX+.225 Y $CY-.225
```

```
'Set the power for the laser

CALL LASERPOWER p5

DWELL $dwelltime +.5

SCOPETRIG

'Set number of pulses and fire the laser

CALL LASERON t($to1) o($to1) k=1 d($dt1)

'Set laser off

CALL LASEROFF

'''

'''Code for coordinate 4:2

'Go to coordinate 4:2

LINEAR X $CX+.075 Y $CY-.225

'Set the power for the laser

CALL LASERPOWER p5

DWELL $dwelltime +.5

SCOPETRIG

'Set number of pulses and fire the laser

CALL LASERON t($to2) o($to2) k=2 d($dt2)
```

```
'Set laser off

CALL LASEROFF

'''

'''Code for coordinate 4:3

'Go to coordinate 4:3

LINEAR X $CX-.075 Y $CY-.225

'Set the power for the laser

CALL LASERPOWER p5

DWELL $dwelltime +.5

SCOPETRIG

'Set number of pulses and fire the laser

CALL LASERON t($to3) o($to3) k=3 d($dt3)

'Set laser off

CALL LASEROFF

'''

'''Code for coordinate 4:4

'Go to coordinate 4:4

LINEAR X $CX-.225 Y $CY-.225
```

```
'Set the power for the laser

CALL LASERPOWER p5

DWELL $dwelltime +.5

SCOPETRIG

'Set number of pulses and fire the laser

CALL LASERON t($to4) o($to4) k=4 d($dt4)

'Set laser off

CALL LASEROFF

"""""""""""""""

'Make sure laser power is set to 0

CALL LASERPOWER p0

CALL LASEROFF

F 10

LINEAR Y -75

END PROGRAM

'''

DFS LASERON

' Configure the pulse generator by setting the pulse on/off times and number of cycles (optional).
```

```
PSOPULSE Z TIME $t, $o 'CYCLES $k

' Specify the output of the PSO to come from the pulse generator.

PSOOUTPUT Z PULSE

' Enable the PSO and force it to fire immediately.

PSOCONTROL Z FIRE

DWELL $d

ENDDFS

DFS LASEROFF

        PSOCONTROL Z OFF

ENDDFS

DFS LASERPOWER

        $AO[0].Z = $p

ENDDFS
```

BIOGRAPHICAL SKETCH

Jesus Gonzalez was born in McAllen, TX on October 7, 1994. He graduated from La Joya High School in La Joya, TX in 2013. He earned a Bachelor of Science Degree in Mechanical Engineering from The Massachusetts Institute of Technology (MIT). Jesus received his Master of Science in Manufacturing Engineering Degree at The University of Texas Rio Grande Valley in December of 2019. He is currently working as an operations engineer in ScanTech Sciences. He can be reached at j.v.gonz345@gmail.com